

# Ground state properties of the mixed-valence cobaltites

$\text{Nd}_{0.7}\text{Sr}_{0.3}\text{CoO}_3$ ,  $\text{Nd}_{0.7}\text{Ca}_{0.3}\text{CoO}_3$  and  $\text{Pr}_{0.7}\text{Ca}_{0.3}\text{CoO}_3$

Z. Jiráček, J. Hejtmánek, K. Knížek, M. Maryško, P. Novák, and E. Šantavá

*Institute of Physics ASCR, Cukrovarnická 10, 162 00 Prague 6, Czech Republic.*

T. Naito and H. Fujishiro

*Faculty of Engineering, Iwate University,*

*4-3-5 Ueda, Morioka 020-8551, Japan.*

## Abstract

The electric, magnetic, and thermal properties of three perovskite cobaltites with the same 30% hole doping and ferromagnetic ground state were investigated down to very low temperatures. With decreasing size of large cations, the ferromagnetic Curie temperature and spontaneous moments of cobalt are gradually suppressed -  $T_C = 130$  K, 55 K and 25 K and  $m = 0.68 \mu_B$ ,  $0.34 \mu_B$  and  $0.23 \mu_B$  for  $\text{Nd}_{0.7}\text{Sr}_{0.3}\text{CoO}_3$ ,  $\text{Pr}_{0.7}\text{Ca}_{0.3}\text{CoO}_3$  and  $\text{Nd}_{0.7}\text{Ca}_{0.3}\text{CoO}_3$ , respectively. The moment reduction with respect to moment of the conventional ferromagnet  $\text{La}_{0.7}\text{Sr}_{0.3}\text{CoO}_3$  ( $T_C = 230$  K,  $m = 1.71 \mu_B$ ) in so-called IS/LS state for  $\text{Co}^{3+}/\text{Co}^{4+}$ , was originally interpreted using phase-separation scenario. Based on the present results, mainly the analysis of Schottky peak originating in Zeeman splitting of the ground state Kramers doublet of  $\text{Nd}^{3+}$ , we find, however, that ferromagnetic phase in  $\text{Nd}_{0.7}\text{Ca}_{0.3}\text{CoO}_3$  and likely also  $\text{Pr}_{0.7}\text{Ca}_{0.3}\text{CoO}_3$  is uniformly distributed over all sample volume, despite the severe drop of moments. The ground state of these compounds is identified with the LS/LS-related phase derived theoretically by Sboychakov *et al.* [Phys. Rev. B **80**, 024423 (2009)]. The ground state of  $\text{Nd}_{0.7}\text{Sr}_{0.3}\text{CoO}_3$  with an intermediate cobalt moment is inhomogeneous due to competing of LS/LS and IS/LS phases. In the theoretical part of the study, the crystal field split levels for  $4f^3$  ( $\text{Nd}^{3+}$ ),  $4f^2$  ( $\text{Pr}^{3+}$ ) and  $4f^1$  ( $\text{Ce}^{3+}$  or  $\text{Pr}^{4+}$ ) are calculated and their magnetic characteristics are presented.

PACS numbers: 71.30.+h;65.40.Ba

Keywords: orthocobaltites; crystal field splitting; metal-insulator transition; spin transitions.

## I. INTRODUCTION

In the perovskite cobaltites, two prototypical behaviors can be distinguished. The first one is associated with spin transition, or spin-state crossover of  $\text{Co}^{3+}$  ions in  $\text{LaCoO}_3$  and its rare earths analogs, while the second one is manifested by robust ferromagnetic metallic ground state that is observed in the mixed-valence  $\text{La}_{1-x}\text{Sr}_x\text{CoO}_3$  systems above a critical doping value of  $x = 0.22$  and exists up to the formally pure  $\text{Co}^{4+}$  end compound  $\text{SrCoO}_3$  [1–3].

It is well established that the ground state of  $\text{LaCoO}_3$  is based on non-magnetic LS (low spin,  $t_{2g}^6$ ) states. With temperature increasing above  $\sim 40$  K the energetically close HS (high spin,  $t_{2g}^4 e_g^2$ ) species start to be populated by thermal excitation. The process is readily seen in the course of magnetic susceptibility or in anomalous terms of lattice expansion due to ionic size of HS notably larger than LS one (see *e.g.* [4]). These experiments show that HS population increases gradually with steepest rate at  $\sim 80$  K, and is practically saturated above 150 K, making about 40 – 50%. Strong HS/LS nearest neighbor correlations or even short-range ordering are anticipated in that phase [5–7]. At still higher temperature the ordering melts, which is accompanied by a drop of the electrical resistivity and thermopower values at about 530 K, reminding the I-M transition. The character of the high-temperature phase is not yet recognized - IS  $\text{Co}^{3+}$  states (intermediate spin,  $t_{2g}^5 e_g^1$ ) have been tentatively suggested [7–9], but very recent LDA+DMFT calculations did not reveal any significant amount of IS  $\text{Co}^{3+}$  in the fluctuating mixture of spin states in  $\text{LaCoO}_3$  at high temperatures [10].

The metallic conductivity in  $\text{La}_{1-x}\text{Sr}_x\text{CoO}_3$  systems with stable ferromagnetic ground state is related to fast valence fluctuations that involve various  $3d^N$  ( $N=5, 6, 7$ ) states on cobalt sites [11]. In particular for  $\text{La}_{0.7}\text{Sr}_{0.3}\text{CoO}_3$ , the dominant population are the IS/LS states for  $\text{Co}^{3+}/\text{Co}^{4+}$ , so that the electronic structure can be approximated as  $t_{2g}^5 \sigma^{*0.7}$ , where  $\sigma^*$  is an antibonding band of the  $e_g$  parentage. This yields spontaneous moment of  $1.70 \mu_B$  in agreement with  $1.71(2) \mu_B$  determined by neutron diffraction (Curie temperature  $T_C = 230$  K) [1, 2]. The spontaneous moment increases with further hole doping, but most of the published data for  $x > 0.5$  are influenced by severe oxygen deficiency of the samples. Nevertheless, nearly pure  $\text{Co}^{4+}$  system  $\text{SrCoO}_3$  has been prepared under very high pressures, yielding the moment of  $2.5 \mu_B$  ( $T_C = 305$  K) [3]. This means that electrons are

not depopulated from the  $e_g$ -derived  $\sigma^*$  band but from the more localized  $t_{2g}$  levels, so that, in gross simplification, the final electronic structure of SrCoO<sub>3</sub> can be presented as  $t_{2g}^4\sigma^{*1}$  (see Ref. [11] for a more detailed description).

As the transition range between LaCoO<sub>3</sub> and La<sub>0.7</sub>Sr<sub>0.3</sub>CoO<sub>3</sub> is concerned, significant data have been obtained in the single crystal studies of He *et al.* [12, 13]. The La<sub>1-x</sub>Sr<sub>x</sub>CoO<sub>3</sub> systems above  $x = 0.22$  show characteristics of conventional ferromagnets. The ferromagnetic-paramagnetic (FM-PM) transition is manifested by large  $\lambda$  peak in the specific heat and by the presence of sharp critical scattering peak in small-angle neutron scattering at  $T_C$ . As shown in recent re-investigation of critical exponents  $\beta$ ,  $\gamma$  and  $\delta$  by Khan *et al.*, the transition is unambiguously of second order, characterized by scaling behavior that belongs to universality class of 3D Heisenberg model [14]. On the contrary, in single crystal samples below  $x = 0.22$  the anomalies at  $T_C$  are absent or smeared out, pointing to a much more complex temperature behavior including the magnetic/electronic phase separation. The magnetic inhomogeneity of low-doped La<sub>1-x</sub>Sr<sub>x</sub>CoO<sub>3</sub> has been proved as well in the inelastic neutron diffraction by Phelan *et al.* [15] or in NMR study by Smith *et al.* [16].

The two regimes of behavior in La<sub>1-x</sub>Sr<sub>x</sub>CoO<sub>3</sub>, separated by the critical doping  $x = 0.22$ , have been interpreted theoretically by Sboychakov *et al.* [17]. Based on a fermionic model of Hubbard type, two possible FM ground states that may coexist on a nanoscopic scale are found. One is derived from the phase characterized by LS/LS state for Co<sup>3+</sup>/Co<sup>4+</sup>, in which only few Co<sup>3+</sup>  $t_{2g}$  electrons promote to itinerant  $e_g$  levels with increasing strontium doping. The second phase is IS/LS state for Co<sup>3+</sup>/Co<sup>4+</sup>, *i.e.* the already mentioned  $t_{2g}^5\sigma^*$  phase, which becomes dominant above the critical composition  $x_c \sim 0.20$ . The model phase diagram presented in Ref. [17] thus reproduce remarkably well the features actually observed in the La<sub>1-x</sub>Sr<sub>x</sub>CoO<sub>3</sub> system.

The properties of mixed-valence cobaltites can be further modified by a control of ionic size on perovskite A sites. Lot of studies have been done on the Pr<sub>1-x</sub>Ca<sub>x</sub>CoO<sub>3</sub> system that exists in a limited range up to  $x \sim 0.55$  [18, 19]. The substitution of smaller Pr<sup>3+</sup> and Ca<sup>2+</sup> ions for La<sup>3+</sup> and Sr<sup>2+</sup> ions causes larger size misfit between the A and B sites of perovskite structure (Goldschmidt's tolerance factor is reduced), which results in larger deviation of the Co-O-Co bond angles from ideal 180° and, subsequently, in narrowing of the  $e_g$ -derived band. The reduced bandwidth is detrimental not only for macroscopic conductivity but also

for ferromagnetic interactions mediated by itinerant  $e_g$  electrons (the double-exchange). Ferromagnetism is thus suppressed and, at the same time, the LS  $\text{Co}^{3+}$  states are promoted due to larger  $t_{2g}-e_g$  gap. As an ultimate effect we may mention the peculiar behavior of  $\text{Pr}_{1-x}\text{Ca}_x\text{CoO}_3$  systems within a range  $x = 0.50 - 0.55$ , which exhibit a sharp first-order transition to the low-temperature highly resistive and weakly magnetic state. It is of interest that the transition is associated with a charge transfer between the cobalt and praseodymium sites, resulting in a stabilization of formally  $\text{Pr}^{4+}$  states - see *e.g.* [20, 21] and references therein. In the region of 30% electron hole doping, to which our study is focused, the pronounced effects of competing ground states were reported for  $\text{Pr}_{0.7}\text{Ca}_{0.3}\text{CoO}_3$ , as well as for  $\text{Nd}_{0.7}\text{Ca}_{0.3}\text{CoO}_3$ , and the phase-separated nature of these compounds was guessed also from the magnetization values, which are severely reduced compared to  $\text{La}_{0.7}\text{Sr}_{0.3}\text{CoO}_3$  ones [22–25].

More direct information on the temperature dependence of magnetic/electronic phase separation was recently provided by the neutron diffraction, small-angle scattering, and magnetometry study of  $\text{Pr}_{0.7}\text{Ca}_{0.3}\text{CoO}_3$  by El-Khatib *et al.* [25]. The study showed that FM clusters (presumably hole-rich objects) were formed at a well-defined temperature  $T^* \sim 250$  K, while the hole-poor PM matrix was transformed to long-range FM order at much lower temperature  $T_C = 70$  K. It is of interest that preformed clusters did not dissolve immediately, but were preserved well below 70 K. This unusual coexistence of short- and long-range ordered FM phases possessing different coercivities was further supported by observation of exchange-spring behavior, which is known for artificial hard-soft magnetic composites [25]. It should be noted that such a behavior refers to a temperature range 50 - 70 K only. The aim of present study is to resolve what is the final magnetic composition in  $\text{Pr}_{0.7}\text{Ca}_{0.3}\text{CoO}_3$  and related compounds at the lowest temperatures.

Our paper reports on the electric, magnetic, and heat capacity investigation of selected 30% doped systems, in decreasing order of tolerance factors  $\text{Nd}_{0.7}\text{Sr}_{0.3}\text{CoO}_3$ ,  $\text{Pr}_{0.7}\text{Ca}_{0.3}\text{CoO}_3$  and  $\text{Nd}_{0.7}\text{Ca}_{0.3}\text{CoO}_3$ . The respective spontaneous moments are determined to  $0.68 \mu_B$ ,  $0.34 \mu_B$  and  $0.23 \mu_B$  ( $T_C = 130$  K, 55 and 25 K). Such drop of magnetization compared to  $1.71 \mu_B$  in  $\text{La}_{0.7}\text{Sr}_{0.3}\text{CoO}_3$  possessing robust IS/LS phase was previously interpreted within the phase separation scenario, supposing that FM ordered regions of higher hole doping are imbedded in the non-magnetic matrix of low hole doping [22–25]. The present results contradict such conjecture. Based on detailed characterization and novel application of

Kramers ions  $\text{Nd}^{3+}$  as local probe of the magnetic ground state, we show that the internal field formed by cobalt spins is uniformly distributed over the sample volume. The presence of gross magnetic/electronic phase separation in  $\text{Nd}_{0.7}\text{Ca}_{0.3}\text{CoO}_3$  or  $\text{Pr}_{0.7}\text{Ca}_{0.3}\text{CoO}_3$  at the lowest temperatures is thus questioned. We argue that the ground state of these samples is in fact the FM saturated LS/LS-derived phase suggested by Sboychakov *et al.* [17].

## II. EXPERIMENTAL

Polycrystalline samples of  $\text{Nd}_{0.7}\text{Sr}_{0.3}\text{CoO}_3$ ,  $\text{Pr}_{0.7}\text{Ca}_{0.3}\text{CoO}_3$  and  $\text{Nd}_{0.7}\text{Ca}_{0.3}\text{CoO}_3$  were prepared using a solid-state reaction. Raw powders of  $\text{Pr}_6\text{O}_{11}$ ,  $\text{Nd}_2\text{O}_3$ ,  $\text{Y}_2\text{O}_3$ ,  $\text{Co}_3\text{O}_4$ ,  $\text{CaCO}_3$  and  $\text{SrCO}_3$  were weighted with proper molar ratios and ground using an agate mortar and pestle for 1 h. Mixed powders were calcinated at  $1000^\circ\text{C}$  for 24 h in air. They were pulverized and ground. Then they were pressed into pellets of 20 mm diameter and 4 mm thickness. Pellets were sintered at  $1200^\circ\text{C}$  for 24 h in 0.1 MPa flowing oxygen gas. The measured densities of each sample were greater than 90% of the ideal density. Powder X-ray diffraction patterns were taken for each sample using  $\text{CuK}_\alpha$  radiation; the samples were confirmed to have a single phase orthoperovskite ( $Pbnm$ ) structure. The lattice parameters and volume *per* f.u. actually obtained are  $a = 5.364 \text{ \AA}$ ,  $b = 5.409 \text{ \AA}$ ,  $c = 7.599 \text{ \AA}$ ,  $V/Z = 55.11 \text{ \AA}^3$  for  $\text{Nd}_{0.7}\text{Sr}_{0.3}\text{CoO}_3$ ,  $a = 5.363 \text{ \AA}$ ,  $b = 5.351 \text{ \AA}$ ,  $c = 7.570 \text{ \AA}$ ,  $V/Z = 54.32 \text{ \AA}^3$  for  $\text{Pr}_{0.7}\text{Ca}_{0.3}\text{CoO}_3$  and  $a = 5.344 \text{ \AA}$ ,  $b = 5.342 \text{ \AA}$ ,  $c = 7.549 \text{ \AA}$ ,  $V/Z = 53.87 \text{ \AA}^3$  for  $\text{Nd}_{0.7}\text{Ca}_{0.3}\text{CoO}_3$ . The present values are in agreement with the literature data for the same compounds [22, 26]. As the important question of the oxygen stoichiometry is concerned, practically ideal oxygen content  $2.99 \pm 0.01$  is evidenced for the  $\text{Pr}_{0.7}\text{Ca}_{0.3}\text{CoO}_3$  specimen by Rietveld refinement of the high resolution neutron diffraction data [27]. The same seems to be valid for other two compounds based on the indirect arguments, which follow from thermopower data presented below.

Electrical resistivity and thermoelectric power were measured using a four-probe method with a parallelepiped sample cut from the sintered pellet. The electrical current density varied in dependence on the sample resistivity between  $10^{-1} \text{ A/cm}^2$  (metallic state) and  $10^{-7} \text{ A/cm}^2$  (insulating state). The measurements were made during cooling and warming the sample. In the low temperature range, the close-cycle cryostat working down to  $2 - 3 \text{ K}$  was used. For the high-temperature experiments up to  $1000 \text{ K}$  the sample was placed on

a ceramic sample holder centered in the small tubular furnace with precisely controlled temperature. The standard chromel-alumel thermocouples were used for monitoring of the temperature gradient around 5 K, imposed across the sample by means of an additional small furnace.

The magnetic measurements were carried out using a SQUID magnetometer MPMS-XL (Quantum Design) in the temperature range 2 – 400 K. The zero-field cooled (ZFC) and field cooled (FC) susceptibilities were measured under different applied fields. The initial AC susceptibility ( $H = 0$ ) was studied in the frequency region 0.12 - 87.4 Hz using a driving AC field 3.9 Oe. The virgin magnetization curves and hysteresis loops (-70 kOe, 70 kOe) in the ZFC regimes were recorded for selected temperatures starting from  $T = 2$  K. In addition to it, the FC hysteresis loops were measured after cooling the sample from  $T = 300$  K to  $T = 2$  K under an applied field 70 kOe.

The specific heat was measured by PPMS device (Quantum Design) using the two- $\tau$  model. The data were collected on sample cooling. The experiments at very low temperatures (down to 0.4 K) were done using the  $^3\text{He}$  option.

### III. RESULTS

#### A. Electric transport

Resistivity data obtained on ceramic samples  $\text{Nd}_{0.7}\text{Sr}_{0.3}\text{CoO}_3$ ,  $\text{Pr}_{0.7}\text{Ca}_{0.3}\text{CoO}_3$  and  $\text{Nd}_{0.7}\text{Ca}_{0.3}\text{CoO}_3$  are presented in the  $\log - \log$  plot in Fig. 1. As the important question on metallic or insulating character of these system is concerned, we argue that bulk properties are generally influenced by the sample granularity, which seems to be also the present case. Namely, the measured resistivity steadily increases with decreasing temperature but, instead of divergence at the lowest temperatures, it extrapolates to finite values of about 1 – 10 m $\Omega$ -cm at zero K, satisfying a criterion for metallic ground state,  $d(\ln\rho)/d(\ln T) \rightarrow 0$  [28]. Another signature for intrinsic metallicity is the apparent activation energy, defined as  $E_A = k \cdot d(\ln\rho)/d(1/T)$ . It does not exceed the thermal energy  $k_B T$ , except for slightly enlarged  $E_A$  values for  $\text{Nd}_{0.7}\text{Ca}_{0.3}\text{CoO}_3$  above  $T_C$  (see the inset of Fig. 1). On the other hand, the thermopower data are rather insensitive to presence of grain boundaries. Seebeck coefficient is positive over the whole temperature range pointing to a hole character of carriers

(Fig. 2). The low-temperature dependence is of linear (metallic-like) type, but tends soon to a maximum at about 150 K, which achieves  $\sim 25, 40$  and  $55 \mu\text{V/K}$  for Nd<sub>0.7</sub>Sr<sub>0.3</sub>CoO<sub>3</sub>, Pr<sub>0.7</sub>Ca<sub>0.3</sub>CoO<sub>3</sub> and Nd<sub>0.7</sub>Ca<sub>0.3</sub>CoO<sub>3</sub>, respectively. Then the thermopower slowly decreases toward a plateau of  $20 \mu\text{V/K}$  at high temperatures. Let us note that the maximum values of thermopower are indirect but very sensitive indicators of the hole doping level and, based on close agreement with data on samples oxygenated under 60 atm pressure in work of Masuda *et al.* [26], they attest oxygen stoichiometry close to the ideal one for our compounds.

The electric properties of Nd<sub>0.7</sub>Sr<sub>0.3</sub>CoO<sub>3</sub>, Pr<sub>0.7</sub>Ca<sub>0.3</sub>CoO<sub>3</sub> and Nd<sub>0.7</sub>Ca<sub>0.3</sub>CoO<sub>3</sub> differ substantially from the behavior of analogously prepared La<sub>0.7</sub>Sr<sub>0.3</sub>CoO<sub>3</sub> ceramics, for which the data have been added to Figs. 1 and 2. First, the resistivity in the La<sub>0.7</sub>Sr<sub>0.3</sub>CoO<sub>3</sub> sample shows a typical metallic dependence with a resistivity drop below  $T_C \sim 220$  K. This becomes still more evident in the graph of the apparent activation energy. More important signature of different ground state is, however, the change of thermopower to negative values at low temperatures, in the case of La<sub>0.7</sub>Sr<sub>0.3</sub>CoO<sub>3</sub> pointing to a dominant role of the electron carriers of  $e_g$  parentage. On the other hand, the above mentioned hole character of thermopower in Nd<sub>0.7</sub>Sr<sub>0.3</sub>CoO<sub>3</sub>, Pr<sub>0.7</sub>Ca<sub>0.3</sub>CoO<sub>3</sub> and Nd<sub>0.7</sub>Ca<sub>0.3</sub>CoO<sub>3</sub> suggests that the transport of  $e_g$  carriers is impeded due to the band narrowing and/or depopulation, and the  $t_{2g}$  band becomes a prevalent conducting channel.

## B. Magnetic properties

The magnetism in presently studied systems is governed by the cobalt spins and their exchange interactions. The contribution of rare earths is manifested by Curie-like susceptibility with effective moments that agree very well with free-ion values at intermediate and high temperatures,  $\mu_{eff} \sim 3.5\mu_B$  both for Nd<sup>3+</sup> and Pr<sup>3+</sup>. However, a significant deviation from this behavior is observed below  $\sim 50$  K, where effects of crystal field splitting on  $4f$  shell become important. The low-temperature properties then depend critically on the character of the rare-earth ground state, which is Kramers doublet for Nd<sup>3+</sup> in the low-symmetry crystal field of perovskite A sites, while the non-Kramers ions Pr<sup>3+</sup> possess a singlet state. This issue is discussed in detail below in Part C and Appendix.

The basic magnetic characterization of Nd<sub>0.7</sub>Sr<sub>0.3</sub>CoO<sub>3</sub>, Pr<sub>0.7</sub>Ca<sub>0.3</sub>CoO<sub>3</sub> and Nd<sub>0.7</sub>Ca<sub>0.3</sub>CoO<sub>3</sub> is represented by the ZFC and FC susceptibilities  $\chi_{ZFC}$ ,  $\chi_{FC}$  mea-



sured in a field of 1000 Oe (Fig. 3). Starting from room temperature both susceptibilities increase with decreasing temperature and the onset of FM phase (Curie temperature) can be specified from an inflection point of the  $\chi_{FC}(T)$  dependence. This yields  $T_C = 130$ , 55 and 25 K for  $\text{Nd}_{0.7}\text{Sr}_{0.3}\text{CoO}_3$ ,  $\text{Pr}_{0.7}\text{Ca}_{0.3}\text{CoO}_3$  and  $\text{Nd}_{0.7}\text{Ca}_{0.3}\text{CoO}_3$ , respectively. With further decreasing of temperature, the  $\chi_{ZFC}$  curves exhibit a maximum at a temperature decreasing with the increasing applied field. The  $\chi_{FC}$  data for  $\text{Pr}_{0.7}\text{Ca}_{0.3}\text{CoO}_3$  increase steadily toward zero temperature, while those for  $\text{Nd}_{0.7}\text{Sr}_{0.3}\text{CoO}_3$  and  $\text{Nd}_{0.7}\text{Ca}_{0.3}\text{CoO}_3$  show a sudden decrease at the lowest temperatures. Such drop is caused by  $\text{Nd}^{3+}$  moments that are induced by FM order in cobalt subsystem and orient antiparallel to  $\text{Co}^{3+}/\text{Co}^{4+}$  spins - see *e.g.* the magnetic and neutron diffraction study of  $\text{Nd}_{1-x}\text{Sr}_x\text{CoO}_3$  sample with  $x = 0.33$  by Krimmel *et al.* [29]. This effect is not seen in  $\text{Pr}_{0.7}\text{Ca}_{0.3}\text{CoO}_3$  sample since the singlet ground state of  $\text{Pr}^{3+}$  lacks intrinsic moment and shows only weak magnetic polarization that arises due to mixing with excited states.

The inverse susceptibility data are presented in a broader range of temperature in Fig. 4. The curvature above  $T_C$ , which is marked for  $\text{Nd}_{0.7}\text{Ca}_{0.3}\text{CoO}_3$  and  $\text{Pr}_{0.7}\text{Ca}_{0.3}\text{CoO}_3$  but hardly visible for  $\text{Nd}_{0.7}\text{Sr}_{0.3}\text{CoO}_3$ , represents a characteristic behaviour for samples with ferrimagnetic ground state. This suggests that not only the Co-Nd but also Co-Pr exchange are of an antiferromagnetic (AFM) kind.

Taking into account the complexity of exchange interactions and crystal field effects, no definite conclusions on the cobalt spin states and their temperature dependence can be drawn from the low-temperature susceptibility data. A simpler situation occurs close to room temperature, where the inverse susceptibility approaches a linear Curie-Weiss behaviour. The slope for  $\text{Nd}_{0.7}\text{Sr}_{0.3}\text{CoO}_3$  gives, after subtraction of free-ion value for  $\text{Nd}^{3+}$  contribution, an effective moment of  $\mu_{eff}^2 \sim 10\mu_B^2$  per Co. This is exactly the theoretical value for IS/IS  $\text{Co}^{3+}/\text{Co}^{4+}$  mixture, which corroborates the results for  $\text{La}_{1-x}\text{Sr}_x\text{CoO}_3$  in the 300 – 600 K range reported by Wu and Leighton [2]. On the other hand, the asymptotic behaviour of high-temperature inverse susceptibility data for  $\text{Pr}_{0.7}\text{Ca}_{0.3}\text{CoO}_3$  and  $\text{Nd}_{0.7}\text{Ca}_{0.3}\text{CoO}_3$  gives notably larger effective moments  $\mu_{eff}^2 \sim 15$  and  $19 \mu_B^2$  per Co, respectively, which may suggest that  $\text{Co}^{3+}$  occur partially in HS state as it is for  $\text{LaCoO}_3$  at the room temperature. This conjecture seems to be supported by observed Weiss temperature  $\theta$  that changes from positive (FM, case of  $\text{Nd}_{0.7}\text{Sr}_{0.3}\text{CoO}_3$ ) to negative (AFM, case of  $\text{Pr}_{0.7}\text{Ca}_{0.3}\text{CoO}_3$  and  $\text{Nd}_{0.7}\text{Ca}_{0.3}\text{CoO}_3$ ) values. With larger disorder, the AFM interactions strengthen as clearly



seen for the  $\text{Nd}_{0.7}\text{Ca}_{0.3}\text{CoO}_3$  sample with yttrium doping, added to Figs. 3 and 4. Although the AFM interactions between cobalt and rare earths may play some role, we relate such drastic change of magnetic interactions at high temperature mainly to the presence of excited HS  $\text{Co}^{3+}$  states in the matrix of dominant LS or IS  $\text{Co}^{3+}$  character.

The behaviour of  $\text{Nd}_{0.7}\text{Ca}_{0.3}\text{CoO}_3$  and  $\text{Nd}_{0.7}\text{Sr}_{0.3}\text{CoO}_3$  in the vicinity of FM transition has been further probed by AC susceptibility, for which real and imaginary parts culminate both near  $T_C$ . For  $\text{Nd}_{0.7}\text{Ca}_{0.3}\text{CoO}_3$  it is clearly seen that the characteristic temperature  $T_f$ , at which the real part  $\chi'$  passes through a maximum, exhibits an upward shift with increasing frequency  $\nu$  of the applied AC field (Fig. 5). In analogy to freezing processes in the spin-glass systems, this shift can be quantified by a semiempirical dimensionless parameter  $K = \Delta T_f / [T_f \Delta(\log \nu)]$ . The value of this parameter was evaluated from the linear approximation of the dependence  $T_f(\log \nu)$  (see the inset of Fig. 5) using the least-squares method, which yields  $K = 0.0095 \pm 0.0005$ . For  $\text{Nd}_{0.7}\text{Sr}_{0.3}\text{CoO}_3$  where frequency shift is less obvious, the analysis gives  $K = 0.0017 \pm 0.0003$ . The existence of a finite frequency shift means that some glassiness or "glassy ferromagnetism" is involved in a broad range below  $T_C$ , and this refers not only to weakly magnetic  $\text{Nd}_{0.7}\text{Ca}_{0.3}\text{CoO}_3$  but also to  $\text{Nd}_{0.7}\text{Sr}_{0.3}\text{CoO}_3$  with stronger FM ground state.

The virgin magnetization curves and ZFC hysteresis loops in fields up to 70 kOe are presented in Fig. 6. The results at the lowest temperatures show a superposition of nearly rectangular hysteresis loop with a linear component that is mostly due to rare-earth contribution. As expected for the magnetic ground state of Kramers ions  $\text{Nd}^{3+}$ , this additional term (paraprocess) is especially large for  $\text{Nd}_{0.7}\text{Sr}_{0.3}\text{CoO}_3$  and  $\text{Nd}_{0.7}\text{Ca}_{0.3}\text{CoO}_3$  while it is much smaller and apparently temperature-independent for  $\text{Pr}_{0.7}\text{Ca}_{0.3}\text{CoO}_3$ . The spontaneous magnetization of Co subsystem, estimated by linear extrapolation to zero field, makes 0.68, 0.34 and 0.23  $\mu_B/\text{Co}$  for  $\text{Nd}_{0.7}\text{Sr}_{0.3}\text{CoO}_3$ ,  $\text{Pr}_{0.7}\text{Ca}_{0.3}\text{CoO}_3$  and  $\text{Nd}_{0.7}\text{Ca}_{0.3}\text{CoO}_3$ , respectively. (In order to eliminate the contribution of  $\text{Nd}^{3+}$  moments in antiparallel alignment, the extrapolation was done using hysteresis curves at higher temperatures, 40 K for  $\text{Nd}_{0.7}\text{Sr}_{0.3}\text{CoO}_3$  and 10 K for  $\text{Nd}_{0.7}\text{Ca}_{0.3}\text{CoO}_3$ , and a small temperature correction of about 5% was applied, based rather arbitrarily on the  $S = 2$  Brillouin function.) Concerning the rare-earth contribution we note that the magnetization curve for  $\text{Nd}_{0.7}\text{Ca}_{0.3}\text{CoO}_3$  at 2 K tends in high fields to a saturation of about 1.3  $\mu_B$  per f.u., which should be interpreted as a sum of  $\mu(\text{Co}) + 0.7\mu(\text{Nd})$ . Since our Brillouin analysis of magnetization curves in a

broader temperature range did not reveal any observable paraprocess of Co subsystem in the  $\text{Nd}_{0.7}\text{Ca}_{0.3}\text{CoO}_3$  sample, we may conclude that the contribution of neodymium moments makes about  $1.0 \mu_B$  or equivalently  $1.4 \mu_B$  per  $\text{Nd}^{3+}$  ion.

The same  $\text{Nd}^{3+}$  moment can be anticipated also for the  $\text{Nd}_{0.7}\text{Sr}_{0.3}\text{CoO}_3$  sample. Here, much higher fields are needed to approach the magnetic saturation, because of stronger AFM coupling between Co and Nd subsystems. Based on a trial measurement at 2 K up to 140 kOe, we have estimated the saturated moment of  $2.3 \mu_B$  per f.u. This may signify that, unlike in  $\text{Nd}_{0.7}\text{Ca}_{0.3}\text{CoO}_3$ , the cobalt moment in  $\text{Nd}_{0.7}\text{Sr}_{0.3}\text{CoO}_3$  increases notably under application of external field, namely from  $0.67 \mu_B/\text{Co}$  at zero field to about  $1.3 \mu_B/\text{Co}$  at 140 kOe. The different behaviour and inhomogeneous character of the  $\text{Nd}_{0.7}\text{Sr}_{0.3}\text{CoO}_3$  sample has been also manifested in a shift of the center of FC hysteresis loop toward negative fields (the exchange bias makes actually 230 Oe at  $T = 2$  K - not shown in Fig. 6a).

### C. The low-temperature specific heat

The specific heat data for all studied samples are presented in a broad temperature range in Fig. 7. The main contribution comes from lattice dynamics, characterized by Debye temperature  $\theta_D \sim 350 - 400$  K for  $\text{Nd}_{0.7}\text{Sr}_{0.3}\text{CoO}_3$ ,  $\text{Pr}_{0.7}\text{Ca}_{0.3}\text{CoO}_3$  and  $\text{Nd}_{0.7}\text{Ca}_{0.3}\text{CoO}_3$ . In addition, there are two contributions that may affect the specific heat values at intermediate temperatures. One is the magnetic term due to cobalt ions, which is manifested by a very weak  $\lambda$  reminding anomaly at  $T_C$  in  $\text{Nd}_{0.7}\text{Sr}_{0.3}\text{CoO}_3$ , but is supposedly spread over larger temperature range in  $\text{Pr}_{0.7}\text{Ca}_{0.3}\text{CoO}_3$  and  $\text{Nd}_{0.7}\text{Ca}_{0.3}\text{CoO}_3$ . The second contribution is due to thermal excitation among the rare-earth  $4f$  electronic levels. In the  $\text{Pr}_{0.7}\text{Ca}_{0.3}\text{CoO}_3$  system with perovskite structure of the orthorhombic  $Pbnm$  symmetry, the  ${}^3\text{H}_4$  electronic multiplet of  $\text{Pr}^{3+}$  is split by crystal field effects to nine singlet levels that are displaced over a large energy range of 100 meV [30]. The thermal population of the first excitation level at about 5 meV is manifested in the specific heat as a broad Schottky-type contribution, onset of which is readily seen as a hump in the  $\text{Pr}_{0.7}\text{Ca}_{0.3}\text{CoO}_3$  data at about 20 K. A more interesting situation is encountered in  $\text{Nd}_{0.7}\text{Sr}_{0.3}\text{CoO}_3$  and  $\text{Nd}_{0.7}\text{Ca}_{0.3}\text{CoO}_3$  where the  ${}^4\text{I}_{9/2}$  multiplet of  $\text{Nd}^{3+}$  is split to five Kramers doublet levels [31]. First, the energy gap between the ground doublet and first excited doublet is larger, 12 meV, so that the relevant Schottky-type contribution is shifted to higher temperatures and becomes more diffusive. Secondly, the

presence of internal field due to FM ordering in cobalt subsystem is responsible for lifting of Kramers degeneracy of  $\text{Nd}^{3+}$  electronic states by Zeeman effects. In particular, the ground level split by internal field is a realization of a standard two-level system for pseudospins  $J' = \pm 1/2$  relevant to two eigenstates of the ground doublet. Their thermal redistribution is reflected by appearance of characteristic Schottky peak in the low-temperature specific heat, see *e.g.* [32, 33]. For present samples, these Schottky peaks and their shift with applied magnetic field are seen in more detail in Fig. 8. In the subKelvin range there is another field-dependent Schottky anomaly of the nuclear ( $^{141}\text{Pr}$ ,  $^{143/145}\text{Nd}$ ,  $^{59}\text{Co}$ ) origin. This  $T^{-2}$  term that is especially strong for  $\text{Pr}_{0.7}\text{Ca}_{0.3}\text{CoO}_3$  (not shown) because of large Van Vleck susceptibility of praseodymium in ground singlet state and strong hyperfine coupling constant.

The profile of the  $\text{Nd}^{3+}$  related Schottky peaks and location on the temperature scale  $\sim 1 - 10$  K are controlled by Zeeman splitting of the ground doublet -  $\Delta E = g_{J'}\mu_B H_{eff}$ , where  $H_{eff}$  is the vector sum of internal and external fields experienced by pseudospins  $J' = \pm 1/2$  in the solid state material. The relevant data, *i.e.* after subtraction of the hyperfine, lattice and linear terms, are displayed as  $c_{Schottky}/T$  vs.  $T$  in Fig. 9. Although the observed curves are broadened with respect to the ideal Schottky peak as exemplified in Fig. 10, no dual distribution of effective fields is found. Macroscopic phase segregation is thus ruled out. Moreover, the observed broadening does not necessarily mean inhomogeneous distribution of effective fields as it can be completely ascribed to anisotropy of  $g_{J'}$ -factor and averaging in polycrystalline samples. The analysis has been actually made supposing an axial symmetry of  $g$ -tensor for the  $\text{Nd}^{3+}$  ground doublet, so that it is described by two components  $g_{\parallel}$  and  $g_{\perp}$  only. This model leads to a modified Schottky form, where the energy splitting  $\Delta E$  for a particular site is given by the angle  $\theta$  corresponding to the deviation of local  $g_{J'}$ -factor axis from the direction of the magnetic field. The partial contribution to the overall Schottky-like anomaly is calculated as  $[(\Delta E_{\parallel} \cos\theta)^2 + (\Delta E_{\perp} \sin\theta)^2]^{1/2}$  and the contribution to specific heat is weighted by  $\sin\theta$ , which corresponds to the random orientation of crystallites in the sample. The fit, represented by solid lines in Figs. 9 and 10, gives for  $\text{Nd}_{0.7}\text{Ca}_{0.3}\text{CoO}_3$  the ratio  $\Delta E_{\parallel}/\Delta E_{\perp} = g_{\parallel}/g_{\perp} \sim 3.0$ , irrespective the strength of applied field. The  $\text{Nd}_{0.7}\text{Sr}_{0.3}\text{CoO}_3$  sample shows at  $H_{ext} = 0$  and 10 kOe an excessive broadening and lower height of Schottky peaks. At higher fields, the curves acquire a similar form and the fit gives a ratio  $\Delta E_{\parallel}/\Delta E_{\perp} = g_{\parallel}/g_{\perp} \sim 4.5$ . As to the absolute values of Zeeman splitting and  $g$ -factors,

the relevant data are plotted in Fig. 11. It is seen that average values of  $\Delta E$  increase with external field in a gradual rate, and only at higher fields a linear dependence is approached. Since the cobalt moments are practically saturated in the Schottky peak range, the final slope seems to be a sole effect of the applied field and can be thus used to determine the  $g_J$ -factor. Average value actually obtained for  $\text{Nd}_{0.7}\text{Ca}_{0.3}\text{CoO}_3$  is  $\langle g_J \rangle = 1.85$ . A similar field dependence is observed also in the plot of nuclear contribution  $\alpha T^{-2}$  for  $\text{Pr}_{0.7}\text{Ca}_{0.3}\text{CoO}_3$ , which probes Van Vleck polarization of  $\text{Pr}^{3+}$  ground singlet.

Turning back to the zero-field values of  $\Delta E = g_J \mu_B H_{eff}$  for  $\text{Nd}_{0.7}\text{Ca}_{0.3}\text{CoO}_3$  and  $\text{Nd}_{0.7}\text{Sr}_{0.3}\text{CoO}_3$  (see Fig. 11), the spontaneous internal field acting on pseudospins can be determined, using the value  $\langle g_J \rangle = 1.85$ , to  $\sim 25$  kOe and 80 kOe, respectively. The last quantity reported here is the entropy change over the Schottky peak, calculated by integration of  $c_{Schottky}/T$ . A value of  $3.95 \pm 0.08$  J·mol $^{-1}$ K $^{-1}$  is obtained for  $\text{Nd}_{0.7}\text{Ca}_{0.3}\text{CoO}_3$ , which is 98% of the theoretical value  $0.7Nk_B \ln 2 = 4.04$  J·mol $^{-1}$ K $^{-1}$ . For  $\text{Nd}_{0.7}\text{Sr}_{0.3}\text{CoO}_3$ , the value obtained from zero-field data makes  $3.45 \pm 0.07$  J·mol $^{-1}$ K $^{-1}$  and increases with increasing applied field to  $3.65 \pm 0.07$  J·mol $^{-1}$ K $^{-1}$ . This corresponds to 85% and 90% of the theoretical value, respectively. The increase with applied field indicates an increasing number of the  $\text{Nd}^{3+}$  pseudospins contributing to Schottky peak. The reduced entropy value at zero field, the large width of Schottky peak showing a gradual narrowing with the applied field, and the magnetic characteristics mentioned above (paraprocess of Co subsystem, finite exchange bias) are signatures of an inhomogeneous FM state in  $\text{Nd}_{0.7}\text{Sr}_{0.3}\text{CoO}_3$ .

#### IV. DISCUSSION

Our structural and electric transport data indicate, that the  $\text{Nd}_{0.7}\text{Sr}_{0.3}\text{CoO}_3$ ,  $\text{Pr}_{0.7}\text{Ca}_{0.3}\text{CoO}_3$  and  $\text{Nd}_{0.7}\text{Ca}_{0.3}\text{CoO}_3$  samples are single-phase highly homogeneous polycrystalline systems of the perovskite  $Pbnm$  structure with oxygen stoichiometry close to the ideal one. As the magnetic characteristics are concerned, a comparison with available literature data on the same cobaltites is worthwhile. Both the saturated magnetic moment  $0.67 \mu_B/\text{Co}$  and  $T_C = 130$  K found for  $\text{Nd}_{0.7}\text{Sr}_{0.3}\text{CoO}_3$  sample are definitely lower compared to  $1.55 \mu_B/\text{Co}$  and 200 K, the data which were reported for chemically most similar  $\text{Nd}_{1-x}\text{Sr}_x\text{CoO}_3$  sample, nonetheless with declared slightly higher Sr content  $x = 0.33$  [29]. Noting that this latter moment value is close to  $1.71 \mu_B$  achieved for  $\text{La}_{0.7}\text{Sr}_{0.3}\text{CoO}_3$ , we pre-

sume that the  $\text{Nd}_{1-x}\text{Sr}_x\text{CoO}_3$  samples with  $x \sim 0.3$  are close to the compositional transition from LS/LS groundstate to IS/LS one. This can explain the large difference in magnetic response between these two samples, despite of their very similar chemical composition. Considering two above mentioned possible ground states, the low critical temperature  $T_C = 25$  K found for our  $\text{Nd}_{0.7}\text{Ca}_{0.3}\text{CoO}_3$  sample can be understood as a fingerprint of a single phase sample with LS/LS FM ground state, while a spin-glass freezing anomaly at much higher temperature of about 55 K reported for the single crystal samples of same composition by Kundu *et al.* can reflect the admixture of the IS/LS ground state with significantly higher  $T_C$  [23]. Simultaneously we rule out a drop of critical temperature due to oxygen deficiency of our sample (see *e.g.* Ref. [22]), since in spite of lower  $T_C$ , we observe a "stronger" FM state with spontaneous moment  $0.23 \mu_B/\text{Co}$  and significant coercivity of  $\sim 10$  kOe at 2 K.

More extensive data are available for the  $\text{Pr}_{0.7}\text{Ca}_{0.3}\text{CoO}_3$  system. Our sample, which oxygen stoichiometry has been proved directly by the neutron diffraction, exhibits FM transition at  $T_C = 55$  K and the spontaneous moment achieves  $0.34 \mu_B/\text{Co}$ . Identical values and similar hysteresis loops were reported for  $\text{Pr}_{0.7}\text{Ca}_{0.3}\text{CoO}_3$  also by Tsubouchi *et al.* [19], while other literature data cluster around higher  $T_C = 70$  K and the magnitude of bulk FM moment is generally lower. The moment of  $0.15 \mu_B/\text{Co}$  for  $\text{Pr}_{0.7}\text{Ca}_{0.3}\text{CoO}_3$  is reported in the above mentioned work of Kundu *et al.* The values found on  $\text{Pr}_{0.7}\text{Ca}_{0.3}\text{CoO}_3$  by El-Khatib *et al.* are  $0.20 \mu_B$  as deduced from magnetization measurements and the long-range ordered moment  $0.30 \mu_B$  *per* f.u. determined by neutron diffraction (this latter value is not explicitly mentioned in the paper, but can be deduced from the graph of magnetic intensities). Cobalt moments of analogous value  $\sim 0.20 \mu_B$  are obtained also by Kalinov *et al.* [24] on  $\text{Pr}_{0.7}\text{Ca}_{0.3}\text{CoO}_3$ -related systems with small A-site substitution by  $\text{Eu}^{3+}$  ions. Importantly, the magnetization curves have been measured up to high fields of 140 kOe, and the data evidence, after subtraction of Pr contribution, a saturation of cobalt magnetization of  $\sim 0.35 \mu_B$  *per* f.u. This value is close to a sole contribution of  $\text{Co}^{4+}$  ions and evidences thus a dominance of LS/LS phase in systems  $\text{Pr}_{0.7}\text{Ca}_{0.3}\text{CoO}_3$  and consequently also  $\text{Nd}_{0.7}\text{Ca}_{0.3}\text{CoO}_3$ .

The most significant results of present study refer to the heat capacity experiments, namely the study and interpretation of the low-temperature Schottky peak associated with  $\text{Nd}^{3+}$  ground state doublet. Using this approach we have demonstrated that presence of rare-earth ions with Kramers degeneracy can be used as a local magnetic probe in mixed-valence cobaltites. Beyond the quantitative information on entropy and level splitting,

it is also possible to analyze the intrinsic or inhomogeneous broadening of the corresponding low temperature Schottky peaks. For this purpose we have performed the theoretical calculations based on the parameters of crystal field, which have been recently deduced from extensive study of terbium aluminate  $\text{TbAlO}_3$  possessing the same  $Pbnm$  perovskite structure [34]. This procedure, described in detail in Appendix, provides not only the necessary characteristic energies of energy level splitting but also the actual form of respective doublet or singlet states. In addition to  $4f^3$  electronic configuration of  $\text{Nd}^{3+}$  and  $4f^2$  for  $\text{Pr}^{3+}$ , the calculations are done also for the  $4f^1$  electronic configuration, which is relevant for the cases of  $\text{Ce}^{3+}$  or  $\text{Pr}^{4+}$ . Turning back to the  $^4I_{9/2}$  multiplet of  $\text{Nd}^{3+}$ , the ground doublet is characterized by highly anisotropic  $g$ -tensor with principal components  $g_x = 4.472$ ,  $g_y = 1.185$  and  $g_z = 0.928$  or, in pseudoaxial approximation  $g_{\parallel}/g_{\perp} \sim 4.2$  (see Table III in Appendix). For enabling a comparison with our experiments, a numerical integration over random orientation of the crystallites has been made, yielding the average value  $\langle g_{J'} \rangle = 2.51$ . This corresponds to the pseudospin moment  $1.255 \mu_B$ , which is in reasonable agreement with the above mentioned saturated magnetization in  $\text{Nd}_{0.7}\text{Ca}_{0.3}\text{CoO}_3$ , giving an estimate of  $1.4 \mu_B$  per  $\text{Nd}^{3+}$  ion. On the other hand, the value  $\langle g_{J'} \rangle = 1.85$  deduced from the high-field shift of Schottky peaks is much lower. An opposite discrepancy has been observed for another Kramers ion  $\text{Pr}^{4+}$  in the low-temperature phase of  $(\text{Pr}_{1-y}\text{Y}_y)_{0.7}\text{Ca}_{0.3}\text{CoO}_3$  with  $y = 0.15$ , where shift of Schottky peaks gives unexpectably large  $\langle g_{J'} \rangle = 3.30$  [33], while calculations in Table II in Appendix give  $\langle g_{J'} \rangle = 2.07$  and a still lower value would be obtained if correction for large  $\text{Pr}^{4+}$  covalency were made. These findings may suggest that apart of the bare interaction of external field with  $4f$  moments, there is an indirect interaction through spin polarizable electronic cloud. The same mechanism likely mediates also the exchange interaction between FM ordered cobalt subsystem and Kramers pseudospins for rare earths, which is of AFM type for  $\text{Nd}^{3+}$  and FM type for  $\text{Pr}^{4+}$  [35].

## V. SUMMARY

The studied mixed-valence cobaltites are systems with complex behaviour. These compounds possess an intrinsic inhomogeneity that relates to chemical and size disorder at the perovskite A-sites, possibility of various spin states at cobalt sites and macroscopic distortion associated with cooperative tilt of  $\text{CoO}_6$  octahedra. With increasing octahedral tilt



(decreasing Goldschmidt's tolerance factor) the FM interactions are suppressed. In particular for  $\text{La}_{0.7}\text{Sr}_{0.3}\text{CoO}_3$ ,  $\text{Nd}_{0.7}\text{Sr}_{0.3}\text{CoO}_3$ ,  $\text{Pr}_{0.7}\text{Ca}_{0.3}\text{CoO}_3$  and  $\text{Nd}_{0.7}\text{Ca}_{0.3}\text{CoO}_3$  with the same 30% doping level, the magnetic Curie temperature gradually decreases,  $T_C = 230$  K, 130 K, 55 K and 25 K, and the spontaneous FM moment on cobalt sites drops,  $1.71 \mu_B$ ,  $0.68 \mu_B$ ,  $0.34 \mu_B$  and  $0.23 \mu_B$ . A difference is also in critical behavior around the magnetic transitions. The  $\text{La}_{0.7}\text{Sr}_{0.3}\text{CoO}_3$  system behaves as conventional ferromagnet. The systems with reduced magnetization show frequency dependent AC susceptibility peaks, pointing to a presence of larger FM clusters for  $\text{Nd}_{0.7}\text{Sr}_{0.3}\text{CoO}_3$  and smaller clusters for  $\text{Nd}_{0.7}\text{Ca}_{0.3}\text{CoO}_3$  or  $\text{Pr}_{0.7}\text{Ca}_{0.3}\text{CoO}_3$  in certain temperature range below  $T_C$ . (A more direct evidence of unusual behaviour in latter systems comes from small angle neutron scattering on  $\text{Pr}_{0.7}\text{Ca}_{0.3}\text{CoO}_3$ , which shows a presence of preformed FM entities of  $10 \text{ \AA}$  size, that only well below  $T_C$  grow to macroscopic size [25].)

The magnetization data on  $\text{Nd}_{0.7}\text{Sr}_{0.3}\text{CoO}_3$ ,  $\text{Pr}_{0.7}\text{Ca}_{0.3}\text{CoO}_3$  and  $\text{Nd}_{0.7}\text{Ca}_{0.3}\text{CoO}_3$  at low temperatures exhibit standard FM hysteresis loops combined with paraprocess caused by rare-earth paramagnetism. The long-range character of magnetic ordering is reported also in few neutron diffraction experiments, which however cannot decide whether severely suppressed moment in  $\text{Pr}_{0.7}\text{Ca}_{0.3}\text{CoO}_3$  and  $\text{Nd}_{0.7}\text{Ca}_{0.3}\text{CoO}_3$  is a manifestation of uniform phase of weakly magnetic character or refers to two-phase coexistence of macroscopic FM and non-magnetic regions [36]. Using the low-temperature heat capacity experiments as an efficient tool for analyzing of internal magnetic fields, we decide in favour of essentially homogeneous phase in the calcium based compounds down to nanoscopic or even atomic scale. First we note that the magnitude of cobalt moments is remarkably close to  $0.3 \mu_B$ , which is exactly the theoretical value for a mixture of non-magnetic  $S = 0$  ions LS  $\text{Co}^{3+}$  and  $S = 1/2$  ions LS  $\text{Co}^{4+}$ . No metamagnetic increase of cobalt magnetization has been detected on application of fields up to 140 kOe. This strongly supports our conclusion that the ground state is the LS/LS phase with only minor promotion of  $t_{2g}$  electrons to itinerant  $e_g$  levels. This promotion is necessarily associated with a rise of cobalt moments, but the increased magnetization might be compensated by presence of oppositely oriented impurity moments due to isolated  $S = 2$  ions HS  $\text{Co}^{3+}$ . Secondly, the form and intensity of Schottky peaks originating in Zeeman splitting of the ground state Kramers doublet of  $\text{Nd}^{3+}$  show unambiguously that all rare-earth sites experience the same effective field. The uniform distribution of hole carriers (formally LS  $\text{Co}^{4+}$ ) in the main LS/LS phase is thus



firmly established for Nd<sub>0.7</sub>Ca<sub>0.3</sub>CoO<sub>3</sub> and can be anticipated for Pr<sub>0.7</sub>Ca<sub>0.3</sub>CoO<sub>3</sub>, as well, in order to account for the similarly reduced magnetization of Co subsystem  $\sim 0.3\mu_B$ . For the remaining compound Nd<sub>0.7</sub>Sr<sub>0.3</sub>CoO<sub>3</sub>, the observed magnetization is intermediate between those for LS/LS in Nd<sub>0.7</sub>Ca<sub>0.3</sub>CoO<sub>3</sub> and IS/LS in La<sub>0.7</sub>Sr<sub>0.3</sub>CoO<sub>3</sub>. Based on a reduced intensity of the Nd<sup>3+</sup>-related Schottky peak, we infer that some rare-earth sites are located in magnetically disordered regions or, to account for exchange bias in Nd<sub>0.7</sub>Sr<sub>0.3</sub>CoO<sub>3</sub>, in AFM ordered regions. Such finding is a direct evidence of inhomogeneous state of this sample.

As a final remark, let us note that present results are closely related to a general problem of the  $3d - 4f$  exchange in perovskite oxides, mediated presumably by spin polarization of extended orbitals of the rare-earth  $5d$  parentage - see the Campbell's indirect exchange mechanism treated in [37] and references therein. It is not yet clear how the mixed valence character of cobaltites, *i.e.* the presence of itinerant carriers, affects the strength and eventually also the sign of exchange interaction. To elucidate all these issues, the magnetic and heat capacity studies on twin-free single crystals are desirable. The single crystal experiments may also give a better test of the homogeneity of FM phases, probed by analysis of the actual form of Schottky peaks, since excessive broadening due to anisotropic  $g$ -factors will be eliminated.

### Appendix A: Electron states and magnetism of lanthanide ions in orthorhombic perovskites

To describe the  $4f$  states of lanthanide ions a Hamiltonian that consists of the free-ion (atomic) and crystal field terms is routinely used:

$$\hat{H} = \hat{H}_a + \hat{H}_{CF}. \quad (\text{A1})$$

The free ion Hamiltonian is spherically symmetrical and in a standard notation (see, for example, Ref. [38]) it can be written as

$$\begin{aligned} \hat{H}_a = E_{avg} + \sum_{k=2,4,6} F^k \hat{f}_k + \zeta_{4f} \sum_{i=1}^N \hat{s}_i \hat{l}_i + \\ \alpha \hat{L}^2 + \beta \hat{G}(G_2) + \gamma \hat{G}(R_2) + \\ \sum_{j=0,2,4} M^j \hat{m}_j + \sum_{k=2,4,6} P^k \hat{p}_k + \sum_{r=2,3,4,6,7,8} T^r \hat{t}(r), \end{aligned} \quad (\text{A2})$$

where  $E_{avg}$  is the energy in central field, terms proportional to  $F^k$ ,  $\alpha, \beta, \gamma$  and  $T^r$  describe the electron-electron interaction, terms with  $\zeta_{4f}$ ,  $M^j$ ,  $P^k$  parameters represent the spin-orbit, spin-other-orbit and electrostatically correlated spin-orbit interactions.  $N$  is number of the  $4f$  electrons.

Within a single electron, crystal field theory the crystal field Hamiltonian may be written as [39]

$$\hat{H}_{CF} = \sum_{k,q,i} B_q^{(k)} \hat{C}_q^{(k)}(i), \quad (\text{A3})$$

where  $\hat{C}_q^{(k)}(i)$  is a spherical tensor operator of rank  $k$  acting on  $i$ th electron and the summation involving  $i$  is over the  $f$  electrons of lanthanide ion.  $B_q^{(k)}$  are crystal field parameters, the values of  $q$  and  $k$  for which they are nonzero depend on the site symmetry and also on the choice of the local coordinate system. The local symmetry of the lanthanide site in orthorhombic perovskites is  $C_s$  and choosing the crystal field coordinate axes along the orthorhombic axes  $a, b, c$  results in three nonzero, real  $B_0^{(k)}$  parameters ( $k = 2, 4, 6$ ) and six nonzero complex  $B_q^{(k)}$  ( $k = 2, 4, 6; q = 2, 4, 6; q \leq k$ ) parameters. Rotation of the crystal field coordinate system around the  $c$  axis allows elimination of the imaginary part of the  $B_2^{(2)}$  parameter (for detailed discussion of the crystal field in orthorhombic perovskites see Ref. [34]). The crystal field axes  $x, y, z$ , ( $z \parallel c$ ) obtained in this way are also principal axes of the lanthanide susceptibility and  $g$  tensor and this system is used in what follows. Low symmetry of the crystal field leads to a complete lift of the orbital degeneracy of  $4f$  levels, so that the states are either singlets ( $N$  even) or Kramers doublets ( $N$  odd).

For the free lanthanide ions the total angular momenta  $L$ ,  $S$ , and  $J$  are good quantum numbers. The ground states are in accord with the Hund's rules and for  $Ce^{3+}$  ( $f^1$ ),  $Pr^{3+}$  ( $f^2$ ) and  $Nd^{3+}$  ( $f^3$ ) they are  ${}^2F_{5/2}$  ( $S=1/2, L=3, J=5/2$ ),  ${}^3H_4$  ( $S=1, L=5, J=4$ ) and  ${}^4I_{9/2}$  ( $S=3/2, L=6, J=9/2$ ), respectively. For a given lanthanide ion the values of parameters of the atomic Hamiltonian (A2) depend to some extent on the host compound. This dependence has little significance for the results given below, however. Decisive for the low temperature behavior of the lanthanide ions is thus the crystal field.

In order to calculate the electron states of trivalent lanthanides in orthorhombic perovskites we used the program 'lanthanide' [40], which makes possible to determine energy levels and eigenfunctions of Hamiltonian (A1) with external magnetic field added. For the atomic parameters values given by Carnall *et al.* [38] were adopted. The crystal parame-

ters  $B_q^{(k)}$  were taken to be the same as those determined recently by Gruber *et al.* [34] for the non-Kramers  $\text{Tb}^{3+}$  ion in terbium aluminate. Eigenenergies and magnetic moments were calculated for the  $4f^8$  electron configuration practically coincides with those obtained by Gruber *et al.* [34]. In particular the energy difference between the lowest two  $\text{Tb}^{3+}$  singlets is only 0.026 meV, very large magnetic moment ( $8.8 \mu_B$  at magnetic field 50 kOe) has an Ising-like character with the Ising axis parallel to the  $x$  axis of the crystal field. There are two crystallographically equivalent sites of  $\text{Tb}^{3+}$  ions in the unit cell related by reflection in the  $ac$  plane. The axis  $x$  for these two sites makes an angle  $\pm 36^\circ$  with the orthorhombic axis  $a$ .

Compared to  $\text{Tb}^{3+}$  the  $\text{Pr}^{3+}$  ion is less anisotropic. The energies and magnetic moments of the states originating from the lowest  $^3H_4$  multiplet of  $\text{Pr}^{3+}$  are given in Table I. The dependence of magnetic moments on magnetic field is to a good approximation linear, only for the first and second excited states and the field parallel to the  $x$  axis there is a tendency to a saturation in high magnetic fields. The induced magnetic moments are small with exception of the first and second excited states that may be classified as Ising-like pseudodoublet. The susceptibility  $\chi$  is anisotropic and its temperature dependence is displayed in Fig. 12.

$\text{Ce}^{3+}$  and  $\text{Nd}^{3+}$  are Kramers ions with  $4f^1$  and  $4f^3$  electron configuration respectively. Magnetic moments of all Kramers doublets are almost field independent: they increase by 1-5% when field changes between 10 and 100 kOe. There is considerable anisotropy of the moment, the  $x$  axis being the easy axis of the ground doublet for both  $\text{Ce}^{3+}$  and  $\text{Nd}^{3+}$ . The  $g$  factors of the Kramers doublets may be determined by multiplying the magnetic moments by factor two, corresponding to a pseudospin 1/2. The calculated energies and the  $g$  factors are summarized in Tables II and III.

**Acknowledgments.** This work was supported by Project No. 204/11/0713 of the Grant Agency of the Czech Republic.

- 
- [1] R. Caciuffo, D. Rinaldi, G. Barucca, J. Mira, J. Rivas, M.A. Señarís-Rodríguez, P.G. Radaelli, D. Fiorani, and J.B. Goodenough, Phys. Rev. B **59**, 1068 (1999).
  - [2] J. Wu and C. Leighton, Phys. Rev. B **67**, 174408 (2003).
  - [3] Y.W. Long, Y. Kaneko, S. Ishiwata, Y. Taguchi, and Y. Tokura, J. Phys.-Condens. Matter

- 23**, 245601 (2011).
- [4] K. Knížek, Z. Jirák, J. Hejtmánek, and P. Novák, *J. Phys.-Condens. Matter* **18**, 3285 (2006).
- [5] J.B. Goodenough, *J. Phys. Chem. Solids* **6**, 287 (1958).
- [6] R.A. Bari and J. Sivardiére, *Phys. Rev. B* **5**, 4466 (1972).
- [7] K. Knížek, Z. Jirák, J. Hejtmánek, P. Novák, and W. Ku, *Phys. Rev. B* **79**, 014430 (2009).
- [8] T. Kyômen, Y. Asaka, and M. Itoh, *Phys. Rev. B* **71**, 024418 (2005).
- [9] Z. Jirák, J. Hejtmánek, K. Knížek, and M. Veverka, *Phys. Rev. B* **78**, 014432 (2008).
- [10] V. Křápek, P. Novák, J. Kuneš, D. Novoselov, D.M. Korotin, and V.I. Anisimov, *Phys. Rev. B* **86**, 195104 (2012).
- [11] J. Kuneš, V. Křápek, N. Parragh, G. Sangiovanni, A. Toschi, and A.V. Kozhevnikov, *Phys. Rev. Lett.* **109**, 117206 (2012).
- [12] C. He, S. El-Khatib, J. Wu, J.W. Lynn, H. Zheng, J.F. Mitchell, and C. Leighton, *Europhys. Lett.* **87**, 027006 (2009).
- [13] C. He, S. Eisenberg, C. Jan, H. Zheng, J.F. Mitchell, and C. Leighton, *Phys. Rev. B* **80**, 214411 (2009).
- [14] N. Khan, A. Midya, K. Mydeen, P. Mandal, A. Loidl, and D. Prabhakaran, *Phys. Rev. B* **82**, 064422 (2010).
- [15] D. Phelan, D. Louca, K. Kamazawa, S.H. Lee, S.N. Ancona, S. Rosenkranz, Y. Motome, M.F. Hundley, J.F. Mitchell, and Y. Moritomo, *Phys. Rev. Lett.* **97**, 235501 (2006).
- [16] R.X. Smith, M.J.R. Hoch, P.L. Kuhns, W.G. Moulton, A.P. Reyes, G.S. Boebinger, J. Mitchell, and C. Leighton, *Phys. Rev. B* **78**, 092201 (2008).
- [17] A.O. Sboychakov, K.I. Kugel, A.L. Rakhmanov, and D.I. Khomskii, *Phys. Rev. B* **80**, 024423 (2009).
- [18] S. Tsubouchi, T. Kyômen, M. Itoh, P. Ganguly, M. Oguni, Y. Shimojo, Y. Morii, and Y. Ishii, *Phys. Rev. B* **66**, 052418 (2002).
- [19] S. Tsubouchi, T. Kyômen, M. Itoh, and M. Oguni, *Phys. Rev. B* **69**, 144406 (2004).
- [20] J. Herrero-Martin, J.L. García-Muñoz, K. Kvashnina, E. Gallo, G. Subias, J.A. Alonso, and A.J. Barón-González, *Phys. Rev. B* **86**, 125106 (2012).
- [21] H. Fujishiro, T. Naito, S. Ogawa, N. Yoshida, K. Nitta, J. Hejtmánek, K. Knížek, and Z. Jirák, *J. Phys. Soc. Jpn.* **81**, 064709 (2012).
- [22] A.K. Kundu, E.V. Sampathkumaran, K.V. Gopalakrishnan, and C.N.R. Rao, *J. Magn. Magn.*

- Mater. **281**, 261 (2004).
- [23] A.K. Kundu, P. Nordblad, and C.N.R. Rao, J. Solid State Chem. **179**, 923 (2006).
- [24] A.V. Kalinov, O.Y. Gorbenko, A.N. Taldenkov, J. Rohrkamp, O. Heyer, S. Jodlauk, N.A. Babushkina, L.M. Fisher, A.R. Kaul, A.A. Kamenev, *et al.*, Phys. Rev. B **81**, 134427 (2010).
- [25] S. El-Khatib, S. Bose, C. He, J. Kuplic, M. Laver, J.A. Borchers, Q. Huang, J.W. Lynn, J.F. Mitchell, and C. Leighton, Phys. Rev. B **82**, 100411 (2010).
- [26] H. Masuda, T. Fujita, T. Miyashita, M. Soda, Y. Yasui, Y. Kobayashi, and M. Sato, J. Phys. Soc. Jpn. **72**, 873 (2003).
- [27] ORNL experiment - to be published later.
- [28] A. Möbius and C.J. Adkins, Physica B **284**, 1669 (2000).
- [29] A. Krimmel, M. Reehuis, M. Paraskevopoulos, J. Hemberger, and A. Loidl, Phys. Rev. B **64**, 224404 (2001).
- [30] A. Podlesnyak, S. Rosenkranz, F. Fauth, W. Marti, H.J. Scheel, and A. Furrer, J. Phys.-Condens. Matter **6**, 4099 (1994).
- [31] A. Podlesnyak, S. Rosenkranz, F. Fauth, W. Marti, A. Furrer, A. Mirmelstein, and H.J. Scheel, J. Phys.-Condens. Matter **5**, 8973 (1993).
- [32] J.E. Gordon, R.A. Fisher, Y.X. Jia, N.E. Phillips, S.F. Reklis, D.A. Wright, and A. Zettl, Phys. Rev. B **59**, 127 (1999).
- [33] J. Hejtmánek, E. Šantavá, K. Knížek, M. Maryško, Z. Jiráček, T. Naito, H. Sasaki, and H. Fujishiro, Phys. Rev. B **82**, 165107 (2010).
- [34] J.B. Gruber, K.L. Nash, R.M. Yow, D.K. Sardar, U.V. Valiev, A.A. Uzokov, and G.W. Burdick, J. Lumines. **128**, 1271 (2008).
- [35] The exchange interaction couples cobalt spins with the spin component of rare-earths moments, which is oppositely oriented to the total momentum in the  $J = L - S$  multiplet. The antiparallel orientation is valid also for projection of spin momentum in Kramers pseudospin  $J'$ .
- [36] In the theoretical case of FM-nonFM phase coexistence, the average value of ordered moment deduced from neutron diffraction is higher than average value deduced from magnetization data (this follows from the fact that magnetic diffraction intensities give a root-square-mean value of moments). This situation seems to occur for Pr<sub>0.7</sub>Ca<sub>0.3</sub>CoO<sub>3</sub> sample probed by El-Khatib *et al.*, but the value  $0.3 \mu_B$  (compared to  $0.2 \mu_B$  obtained by magnetization method)

is close to the resolution limit of neutron diffraction and is thus subjected to large uncertainty.

- [37] M. Richter, J. Phys. D-Appl. Phys. **31**, 1017 (1998).
- [38] W.T. Carnall, G.L. Goodman, K. Rajnak, and R.S. Rana, J. Chem. Phys. **90**, 3443 (1989).
- [39] B.G. Wybourne, *Spectroscopic Properties of Rare Earth* (Interscience, New York, 1965).
- [40] S. Edvardsson and D. Aberg, Comput. Phys. Commun. **133**, 396 (2001).

TABLE I: States of the ground  ${}^3H_4$  multiplet of  $\text{Pr}^{3+}$  ion split by the crystal field. Energy, relative to the ground state, at zero external magnetic field, and the magnetic moments  $m_x$ ,  $m_y$ ,  $m_z$ , induced by field of 10 kOe.

state	$E$ [meV]	$m_x$ [ $\mu_B$ ]	$m_y$ [ $\mu_B$ ]	$m_z$ [ $\mu_B$ ]
1	0.00	0.0469	0.0308	0.0139
2	8.29	0.2765	0.0536	-0.0021
3	9.94	-0.2484	-0.0182	0.0514
4	11.57	-0.0667	-0.0302	-0.0431
5	27.57	0.0620	0.0321	0.0144
6	29.98	-0.0624	-0.0407	-0.0038
7	52.92	0.0073	0.0041	-0.0216
8	63.61	-0.0052	-0.0250	0.0743
9	74.20	-0.0081	-0.0043	-0.0811

TABLE II: Three Kramers doublets of the ground  ${}^2F_{5/2}$  multiplet of  $\text{Ce}^{3+}$  ion split by the crystal field. Energy, relative to the ground state, at zero external magnetic field, and the  $g$  factors.

state	$E$ [meV]	$g_x$	$g_y$	$g_z$
1	0.00	3.757	0.935	0.606
2	33.46	1.298	2.298	1.458
3	56.36	0.945	1.212	3.451

TABLE III: Five Kramers doublets of the ground  ${}^4I_{9/2}$  multiplet of  $\text{Nd}^{3+}$  ion split by the crystal field. Energy, relative to the ground state, at zero external magnetic field, and the  $g$  factors.

state	$E$ [meV]	$g_x$	$g_y$	$g_z$
1	0.00	4.472	1.185	0.928
2	11.83	0.942	3.925	1.077
3	22.87	2.034	1.257	3.540
4	53.52	2.978	3.063	1.052
5	65.33	1.788	1.435	4.204



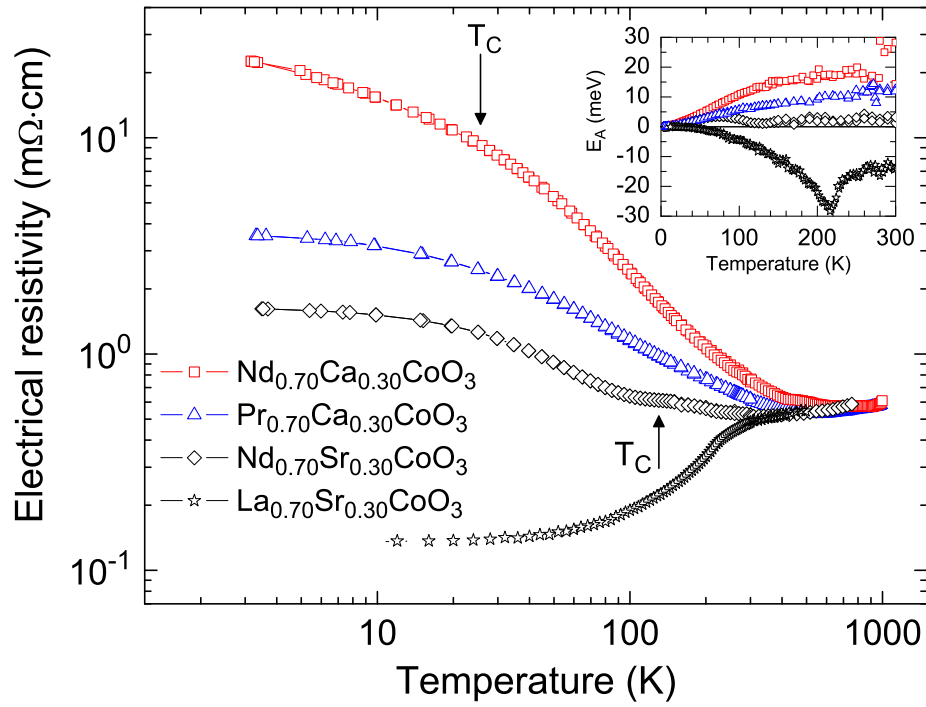


FIG. 1: (Color online) Resistivity of the Nd<sub>0.7</sub>Sr<sub>0.3</sub>CoO<sub>3</sub>, Pr<sub>0.7</sub>Ca<sub>0.3</sub>CoO<sub>3</sub> and Nd<sub>0.7</sub>Ca<sub>0.3</sub>CoO<sub>3</sub> ceramic samples. Results on La<sub>0.7</sub>Sr<sub>0.3</sub>CoO<sub>3</sub> ceramics are added for comparison. The inset shows that, except for Nd<sub>0.7</sub>Ca<sub>0.3</sub>CoO<sub>3</sub>, the apparent activation energy, defined as  $E_A = k \cdot d(\ln \rho) / d(1/T)$ , is below the thermal energy in the whole temperature range (the full line refers to  $kT$ ).

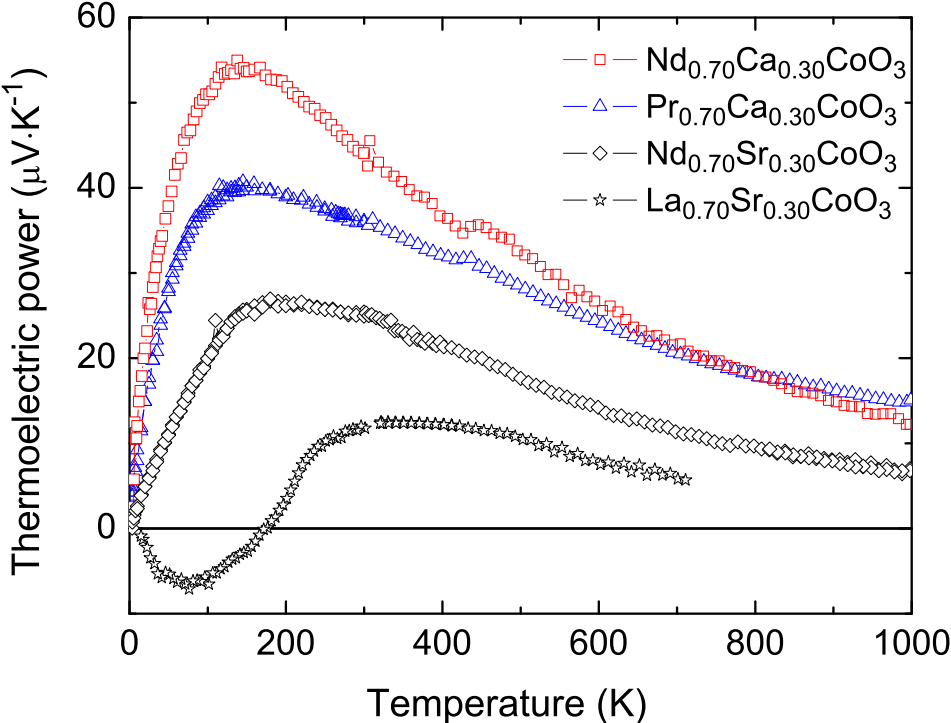


FIG. 2: (Color online) The thermopower data of  $\text{Nd}_{0.7}\text{Sr}_{0.3}\text{CoO}_3$ ,  $\text{Pr}_{0.7}\text{Ca}_{0.3}\text{CoO}_3$ ,  $\text{Nd}_{0.7}\text{Ca}_{0.3}\text{CoO}_3$  and  $\text{La}_{0.7}\text{Sr}_{0.3}\text{CoO}_3$ .

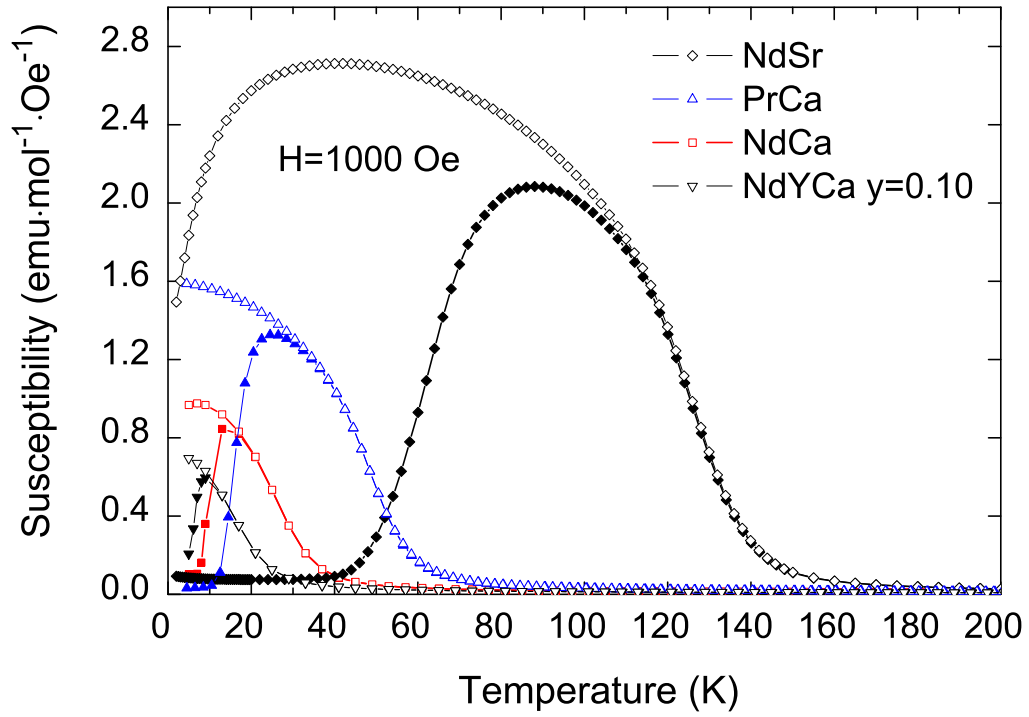


FIG. 3: (Color online) The zero-field-cooled (full symbols) and field-cooled (open symbols) curves of DC susceptibility in  $\text{Nd}_{0.7}\text{Sr}_{0.3}\text{CoO}_3$ ,  $\text{Pr}_{0.7}\text{Ca}_{0.3}\text{CoO}_3$  and  $\text{Nd}_{0.7}\text{Ca}_{0.3}\text{CoO}_3$ , measured at field of 1000 Oe. The effect of an additional disorder is demonstrated by the data of  $(\text{Nd}_{1-y}\text{Y}_y)_{0.7}\text{Ca}_{0.3}\text{CoO}_3$  ( $y = 0.10$ ).

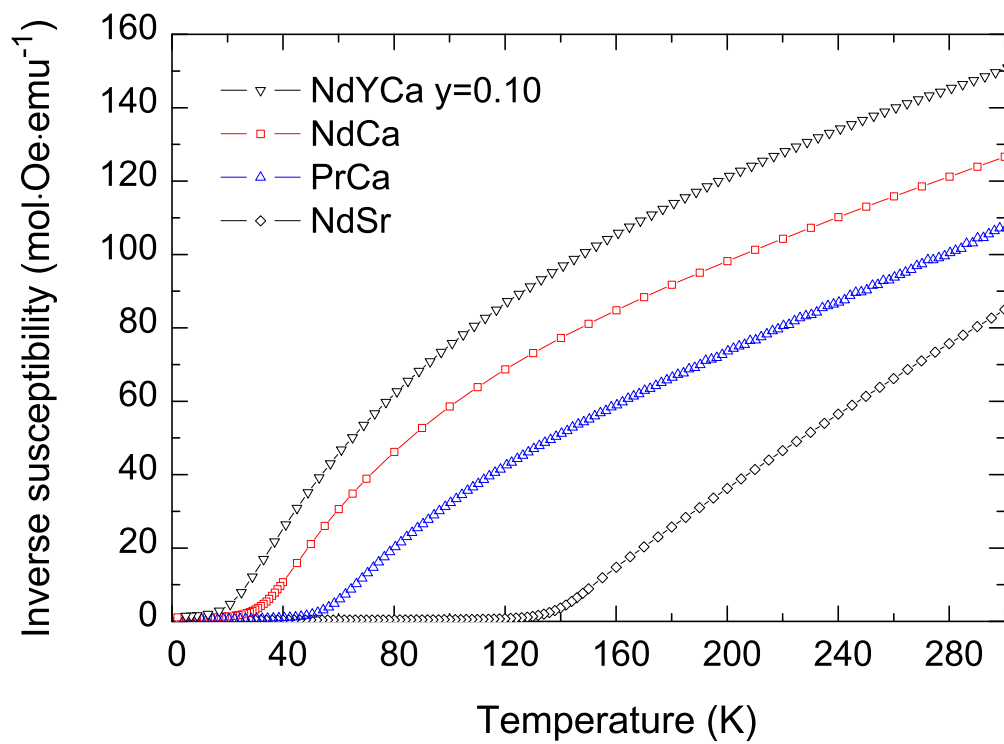


FIG. 4: (Color online) The inverse susceptibility for  $\text{Nd}_{0.7}\text{Sr}_{0.3}\text{CoO}_3$ ,  $\text{Pr}_{0.7}\text{Ca}_{0.3}\text{CoO}_3$ ,  $\text{Nd}_{0.7}\text{Ca}_{0.3}\text{CoO}_3$  and  $(\text{Nd}_{1-y}\text{Y}_y)_{0.7}\text{Ca}_{0.3}\text{CoO}_3$  ( $y = 0.10$ ), based on FC data.

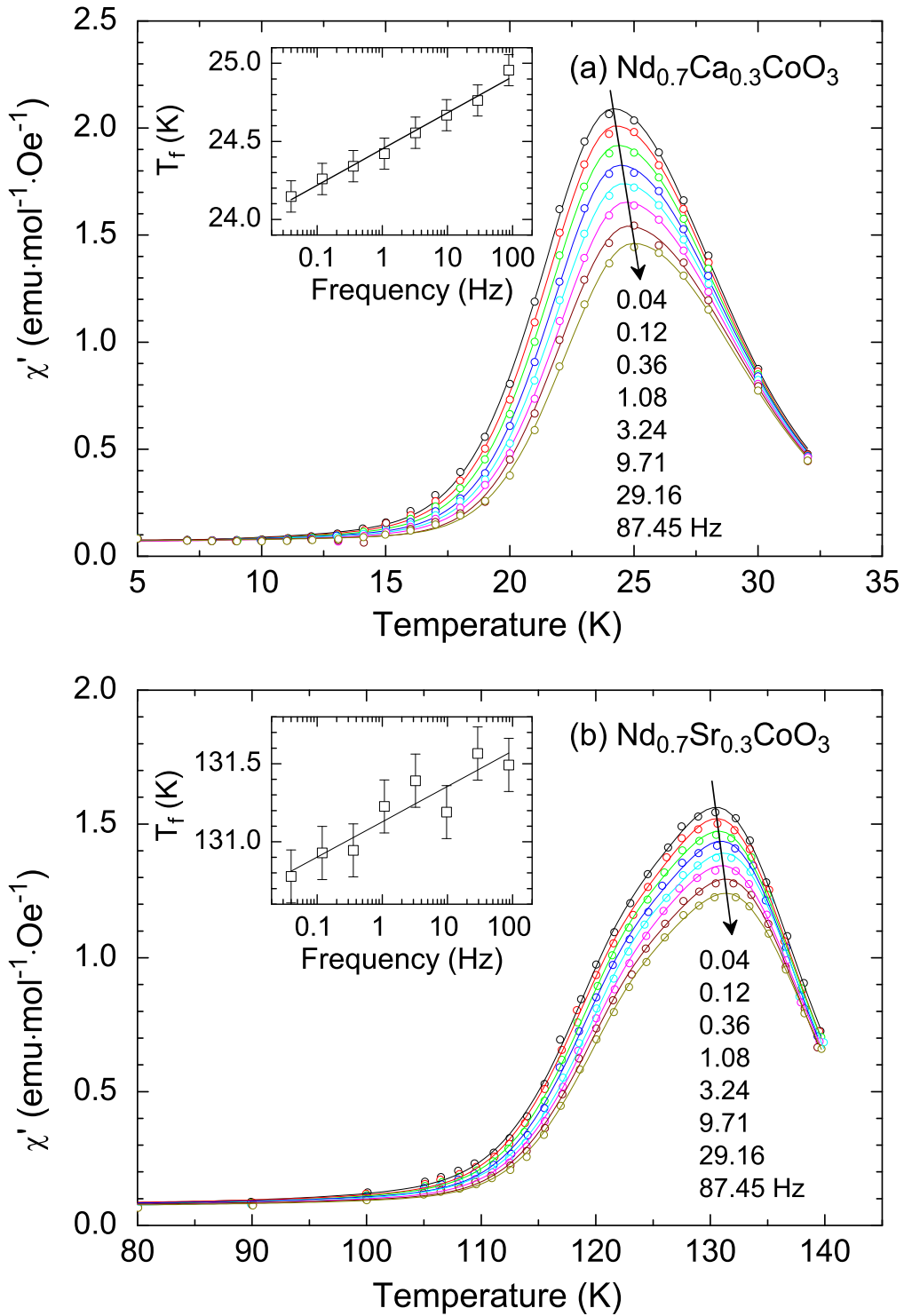


FIG. 5: (Color online) The real part of AC susceptibility for  $\text{Nd}_{0.7}\text{Ca}_{0.3}\text{CoO}_3$  and  $\text{Nd}_{0.7}\text{Sr}_{0.3}\text{CoO}_3$ . The experimental data are marked by the symbols; the full lines represent the least-squares fit of the peak form. The inset shows the frequency dependence of freezing temperature  $T_f$ , corresponding to the susceptibility maximum.

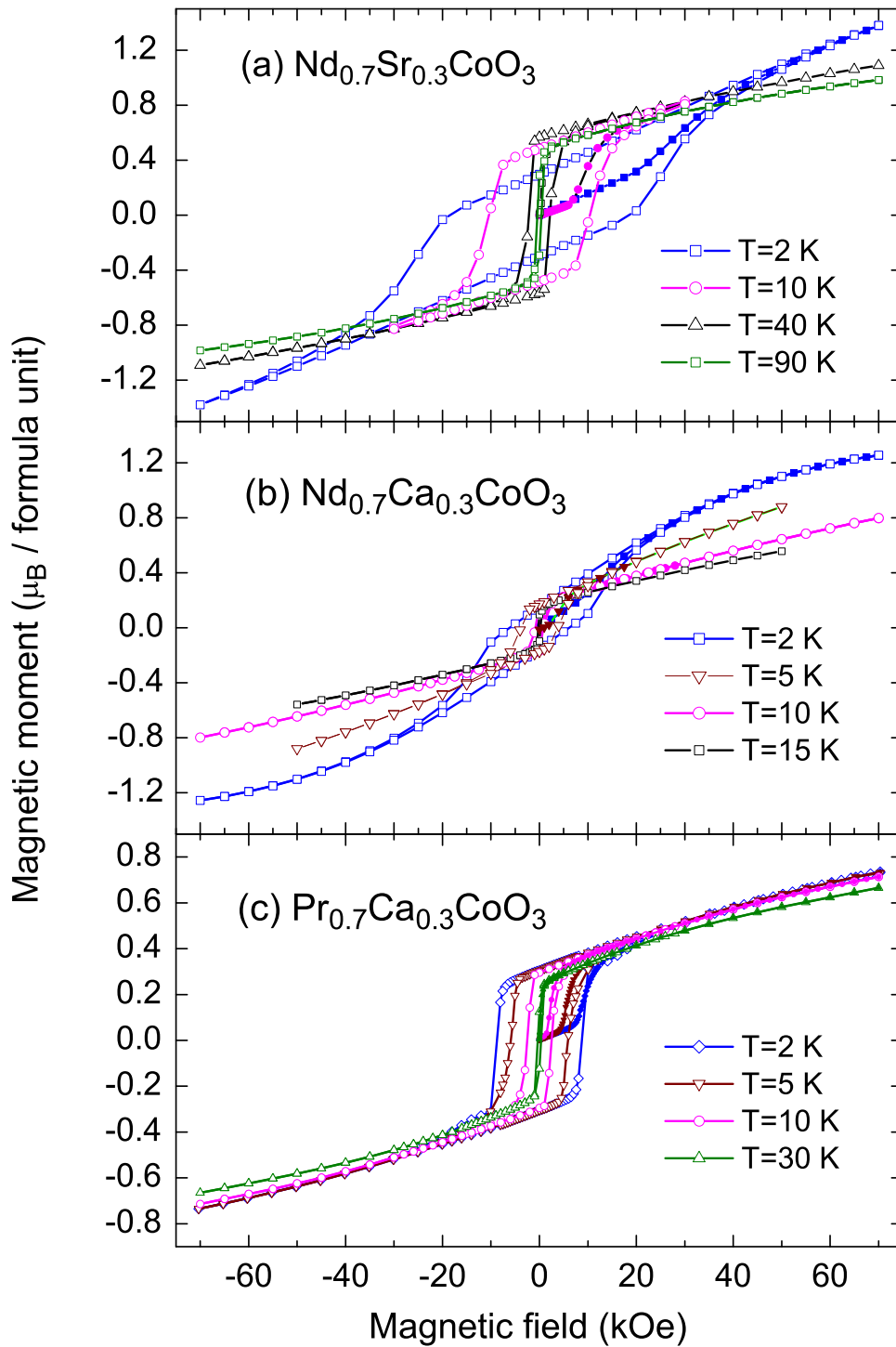


FIG. 6: (Color online) The virgin magnetization curves and ZFC hysteresis loops for  $\text{Nd}_{0.7}\text{Sr}_{0.3}\text{CoO}_3$  (a),  $\text{Nd}_{0.7}\text{Ca}_{0.3}\text{CoO}_3$  (b) and  $\text{Pr}_{0.7}\text{Ca}_{0.3}\text{CoO}_3$  (c), taken at selected temperatures between  $T_C$  and 2 K.

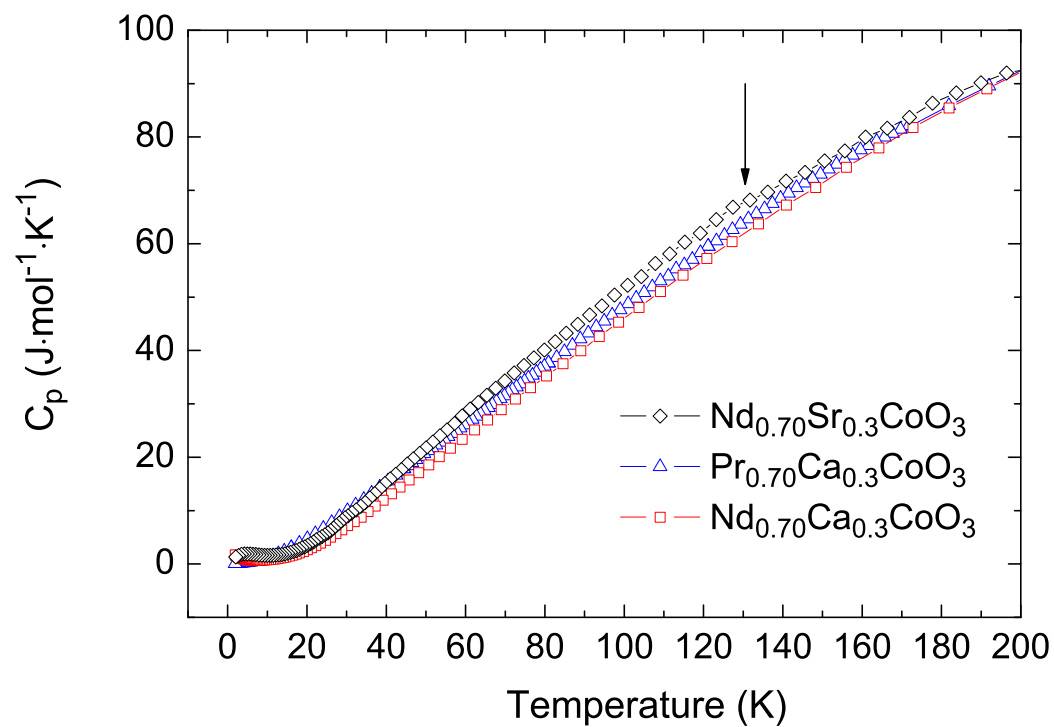


FIG. 7: (Color online) The heat capacity of  $\text{Nd}_{0.7}\text{Sr}_{0.3}\text{CoO}_3$ ,  $\text{Pr}_{0.7}\text{Ca}_{0.3}\text{CoO}_3$  and  $\text{Nd}_{0.7}\text{Ca}_{0.3}\text{CoO}_3$  at intermediate temperatures. The arrow marks a weak anomaly at  $T_C$  for  $\text{Nd}_{0.7}\text{Sr}_{0.3}\text{CoO}_3$ .



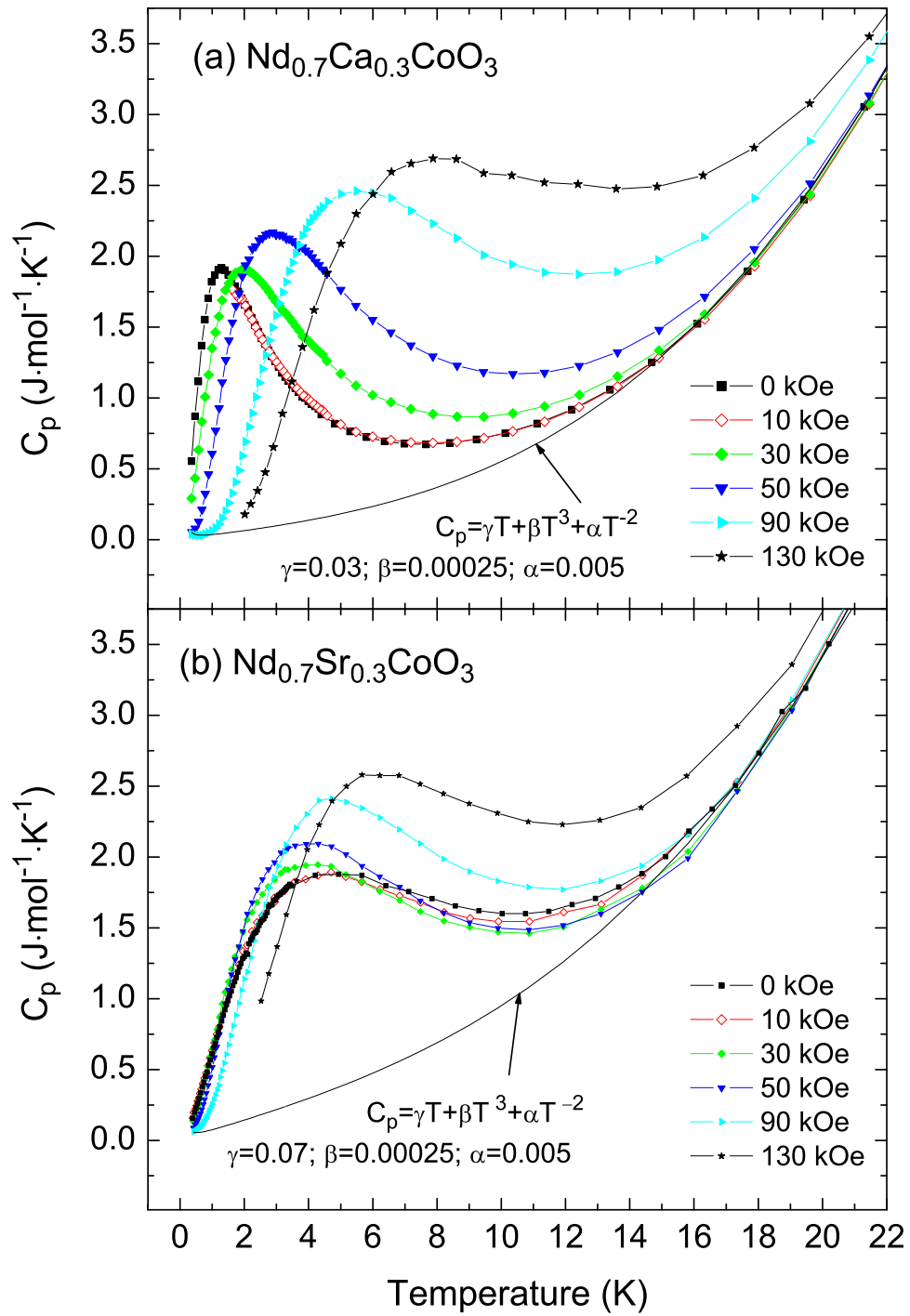


FIG. 8: (Color online) The low-temperature heat capacity of  $\text{Nd}_{0.7}\text{Ca}_{0.3}\text{CoO}_3$  and  $\text{Nd}_{0.7}\text{Sr}_{0.3}\text{CoO}_3$ . The background line corresponding to a contribution of the hyperfine, lattice and linear terms is estimated with relative uncertainty of about 5%, which reflects some ambiguity of the  $\alpha$ ,  $\beta$  and  $\gamma$  parameters.

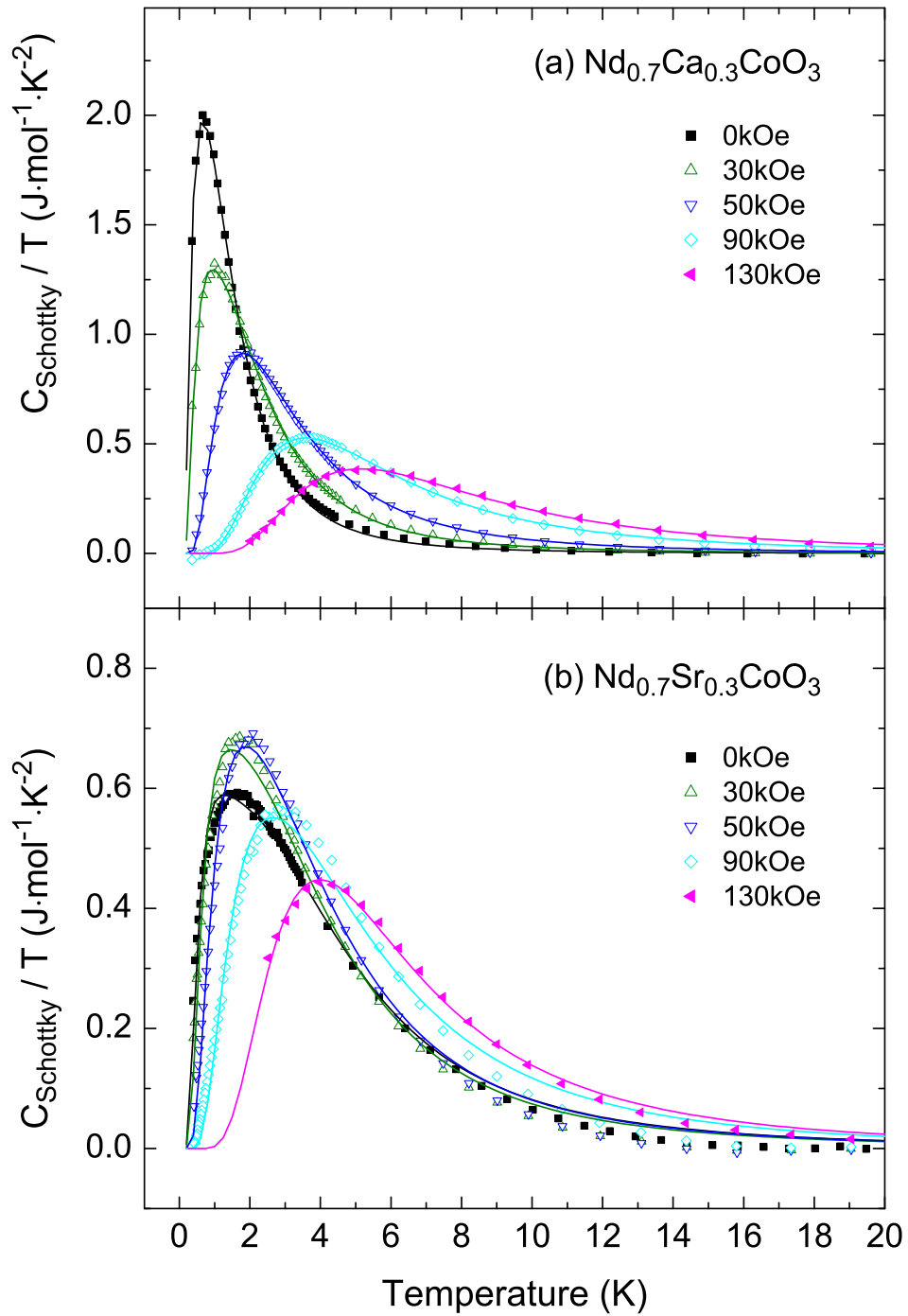


FIG. 9: (Color online) The heat capacity divided by temperature for  $\text{Nd}_{0.7}\text{Ca}_{0.3}\text{CoO}_3$  and  $\text{Nd}_{0.7}\text{Sr}_{0.3}\text{CoO}_3$ , after subtraction of lattice and nuclear terms. The full lines present the theoretical fit based on the broadening due to anisotropic Zeeman splitting.

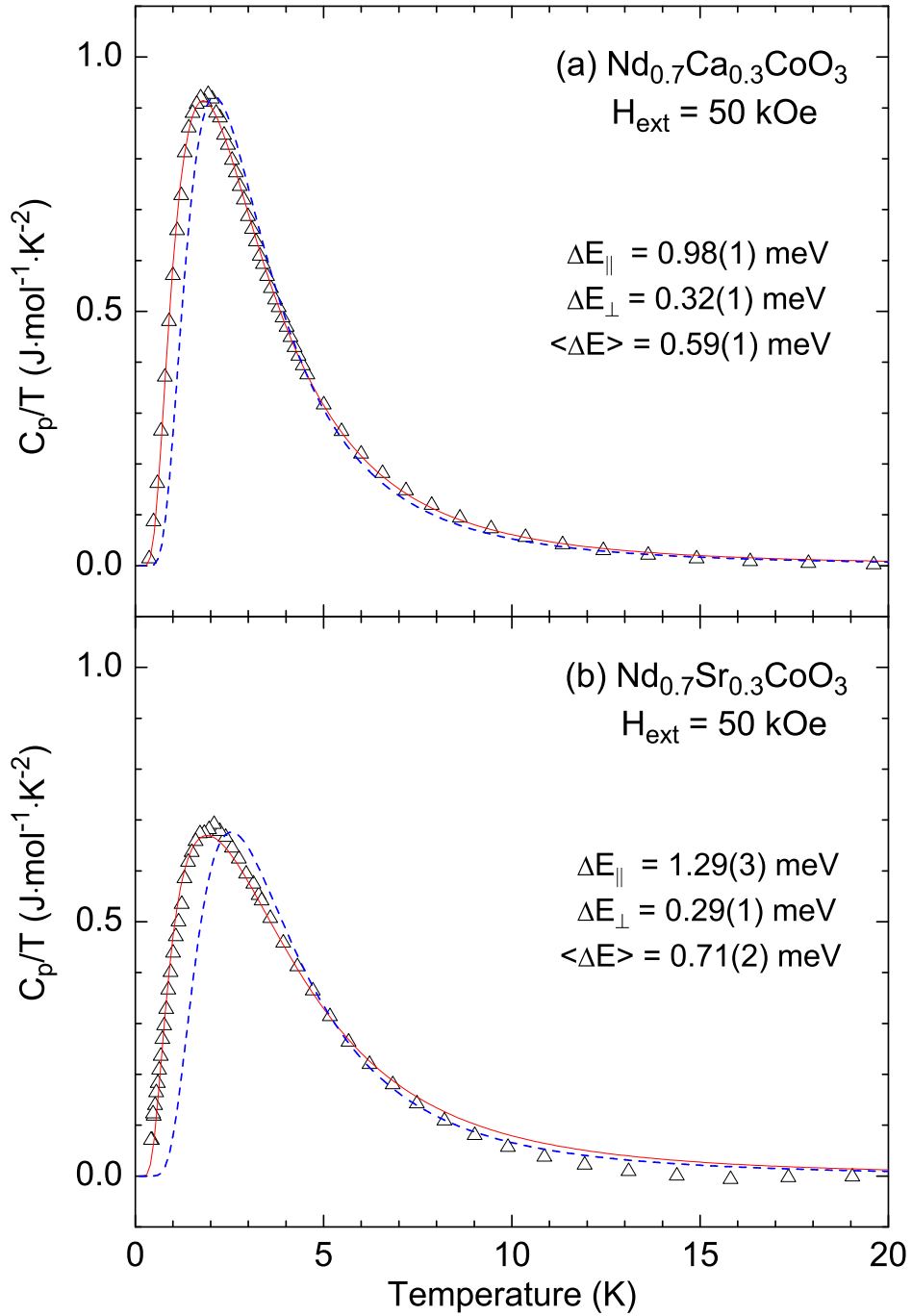


FIG. 10: (Color online) The  $c_{Schottky}$  contribution to the low-temperature heat capacity of Nd<sub>0.7</sub>Ca<sub>0.3</sub>CoO<sub>3</sub> and Nd<sub>0.7</sub>Sr<sub>0.3</sub>CoO<sub>3</sub> at  $H_{ext} = 50$  kOe. The experimental peaks and their fitted profiles in model of anisotropic  $\Delta E$  are compared with the theoretical form for ideal Schottky peak (the dashed line), which would correspond to isotropic model with the same entropy change and splitting  $\langle \Delta E \rangle$ .

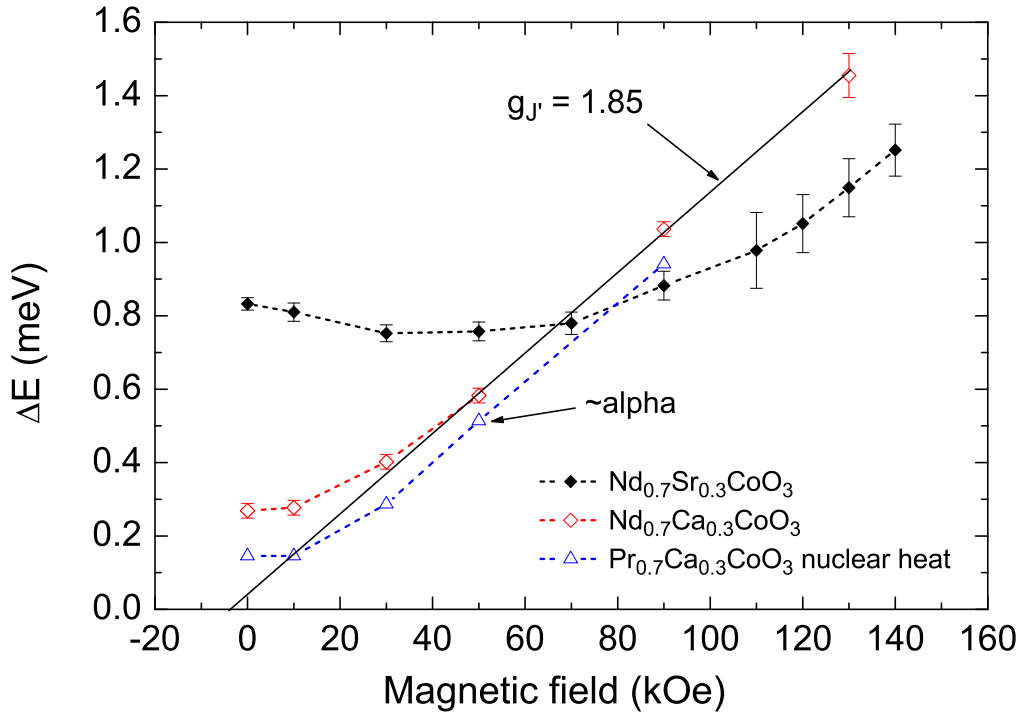


FIG. 11: (Color online) Average Zeeman splitting of the  $\text{Nd}^{3+}$  ground doublet for  $\text{Nd}_{0.7}\text{Ca}_{0.3}\text{CoO}_3$  and  $\text{Nd}_{0.7}\text{Sr}_{0.3}\text{CoO}_3$ . The linear behaviour for  $\text{Nd}_{0.7}\text{Ca}_{0.3}\text{CoO}_3$  above  $H_{ext} = 50$  kOe gives  $\langle g_J \rangle = 1.85$ . Similar dependence is observed also for the nuclear term  $\alpha \cdot T^{-2}$  in  $\text{Pr}_{0.7}\text{Ca}_{0.3}\text{CoO}_3$ . The parameter  $\alpha$ , which is proportional to hyperfine field induced by Van Vleck susceptibility of the  $\text{Pr}^{3+}$  electronic singlet, achieves the values  $0.0034 \text{ J}\cdot\text{K}\cdot\text{mol}^{-1}$  and  $0.0220 \text{ J}\cdot\text{K}\cdot\text{mol}^{-1}$  for  $H_{ext} = 0$  and 90 kOe, respectively.

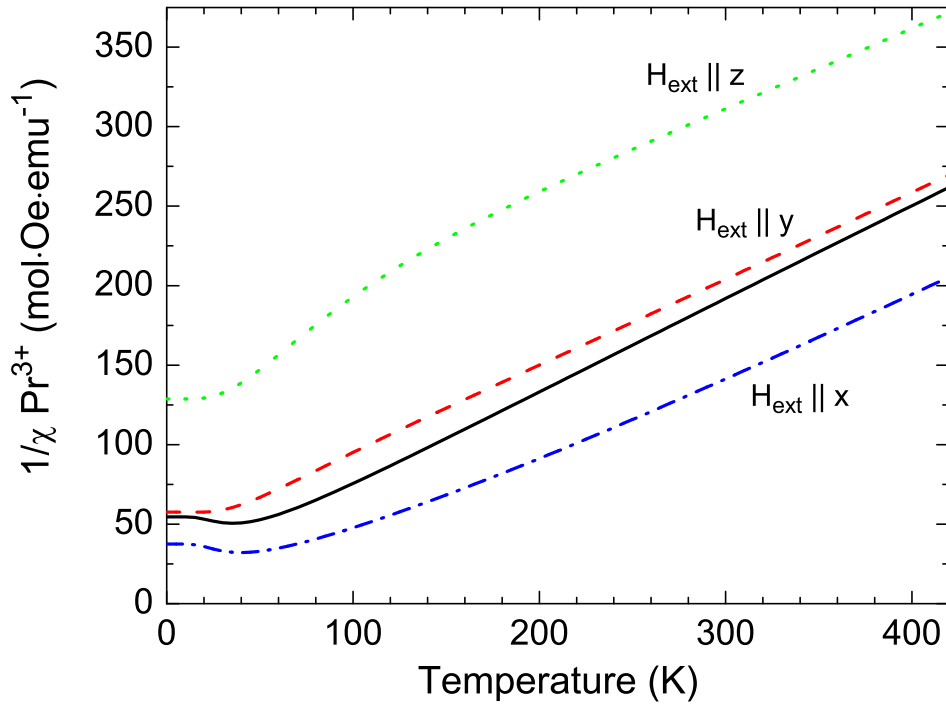


FIG. 12: (Color online) Theoretical dependence of the inverse susceptibility of Pr<sup>3+</sup> ion, based on the singlet state energies in Table I and the calculated shifts in field of 10 kOe. The full line corresponds to the average over random orientations; the linear Curie behavior at higher temperatures gives an effective moment of  $\mu_{eff} = 3.68\mu_B$  in agreement with the experimental value  $\sim 3.5\mu_B$ .